Geochronology and geochemistry of exotic clasts of Cadomian crust from the salt diapirs of SE Zagros: The Chah-Banu Salt Diapir Example

Abstract

Cadomian calc-alkaline I-type and within-plate A-type rocks are widespread in the crust of Iran where they are ascribed to the southward subduction of Prototethyan oceanic lithosphere beneath N Gondwana. These rocks are present as unmetamorphosed magmatic rocks and/or their metamorphic equivalents (mafic to felsic gneisses) and could be generated in both Cadomian arcs and associated rear-arcs. Nearly all these exposures contain metamorphosed metasediments, whereas in central Iran, Cadomian igneous rocks are associated with thick sequences of unmetamorphosed terrigenous rocks. In the Zagros Fold-Thrust belt of S Iran, salt domes contain abundant Cadomian igneous and sedimentary rocks as xenoliths in association with evaporites, dolomites, carbonates and banded iron-salt deposits. This paper presents new zircon U-Pb as well as geochemical-isotopic data from igneous clasts in Chah-Banu salt diapir in SE Zagros. Petrographic and geochemical data indicate two different types of rock clasts; calc-alkaline, I-type dacites-rhyolites and E-MORB to OIB-like gabbros, basalts and dolerites. New zircon U-Pb ages show that dacites formed at 538.2±2.2, whereas gabbros show ages of 539.0±1.8 Ma. Zircons from dacites have negative εHf(t) values of –1.1 to –8.3, suggesting significant contribution of crustal components in the melt source of these rocks, or during the melt ascent and emplacement. In contrast, zircons from gabbros have higher εHf(t) values of +4.5 to +8.5, indicating that mantle-derived juvenile magmas were responsible for these magmas. Bulk rock Nd-Sr isotopic data (e.g., εNd(t)= +0.3 to +4.0 and $^{87}Sr/^{86}Sr_{(i)}$ =0.7059 to 0.70848) for gabbros, dolerites and basalts confirm that these rocks originated from an enriched mantle source similar to subcontinental lithospheric mantle, whereas dacites and rhyolites (with εNd(t) = −3.4 to −4.1 and $^{87}Sr/^{86}Sr_{(i)}$ =0.70806 to 0.70907) show strong interaction with, and/or re-melting of a continental crust. We suggest that the bimodal calc-alkaline and OIB-like magmatic rocks in salt domes as well as associated evaporites and sedimentary rocks formed in a retro-arc rifted basin behind the Cadomian magmatic arc.

1. Introduction

The Neoproterozoic is a well-documented time of enhanced juvenile crust formation, especially in the Arabian-Nubian Shield (Stern et al. 2012). Cryogenian crust formation was followed by Ediacaran continental collision between fragments of E and W Gondwana to form a "Greater Gondwana" supercontinent. The northern margin of Greater Gondwana developed a Late Ediacaran-Early Cambrian active margin (Zulauf et al. 1997; Crowley et al. 2000). This belt can be traced from eastern North America to Iberia through central and southern Europe into the eastern Mediterranean region, Turkey, Iran and perhaps further into Central Asia (von Raumer et al. 2002). Cadomian-Avalonian fragments rifted from northern Gondwana during the Paleozoic and accreted to Laurasia at various times. The geodynamic evolution documented in the magmatic and sedimentary record of this region is related to subduction of two Paleozoic oceanic basins: The Iapetus and Rheic oceans. Because Cadomian fragments rifted away from northern Gondwana, the paleogeography of the Late Ediacaran-Early Cambrian active margin of Gondwana is not fully understood and has been debated for several decades (e.g., (Nance & Murphy 1994; Neubauer et al. 2001; Ustaomer et al. 2009; Pereira et al. 2011; Linnemann et al. 2014; Abbo et al. 2015; Shafaii Moghadam et al. 2020)).

The geology of SW Asia reflects a long and complex tectonic history that reflects the collision and accretion of several peri-Gondwanan blocks to the Eurasian margin (Angiolini et al. 2013). The Cimmerian continental blocks of Iran separated from northern Gondwana in Permian time and collided with Eurasia during Late Triassic time. These Cadomian continental blocks preserve evidence of peri-Gondwanan intra-continental magmatism, deformation, metamorphism and sedimentation from at least Late Neoproterozoic (Ediacaran) until detachment from Gondwana in Permian time. Recent studies increasingly focus on the Cadomian basement of Anatolia and Iran, mostly on the granitic rocks and equivalent gneisses.

Cadomian rock exposures are abundant in Iran and occur in the NW (Khoy-Salmas, Takab-Zanjan), NE (Torud-Taknar), central (Saghand-Golpayeagn) and SE (Zarand) (Fig. 1A). In addition, there are many salt diapirs in SE Iran which contain gigantic to small-sized exotic blocks/clasts of Cadomian igneous, metamorphic and sedimentary rocks. These salt diapirs are widespread in the SE Zagros Fold-Thrust Belt (ZFTB) and are part of the Persian Gulf salt basin (Fig. 1B). Salt basins are also abundant in SE segments of Persian Gulf, in Oman and include Fahud-, Ghaba- and south Oman salt basins (Fig. 1B). There are only few studies of the rock clasts within these salt-domes, but their ages and geochemical signatures are important for the reconstructing the Cadomian tectono-magmatic evolution of Iran (e.g., (Alavi 2004; Faramarzi et al. 2015)). This paper aims to fill some of these gaps by studying Cadomian exotic clasts recovered from a salt diapir in SE Zagros.

More than 200 salt diapirs have been identified in the S-SE Zagros Fold-Thrust Belt (ZFTB) and Iranian Persian Gulf areas (e.g., (Edgell 1991; Talbot et al. 2009a; Talbot et al. 2009b)). These salt diapirs are sourced from a thick sequence of deeply buried Ediacaran-Cambrian evaporites; the Hormuz series (Husseini 1992; Talbot & Alavi 1996; Thomas et al. 2015). Hormuz series is composed of different lithologies and origin but contain abundant Cadomian exotic clasts. The Hormuz series is similar to the Ediacaran-Cambrian Ara group evaporites and dolostones along with Fara volcanic and Nimr siliciclastic rocks- which constitute younger members of the Cryogenian-Cadomian Huqf Supergroup of Oman (Bowring et al. 2007).

The Ara evaporites include 10-20 m thick anhydrites and hundreds of meters thick halites and potash salts along with volcanic tuffs (Mattes & Morris 1990). Tuffaceous carbonates from the Ara Group display two age clusters at 546.7 and 548.9 Ma (Bowring et al. 2007). The Fara Formation of Oman consists three lithologies including; a lower unit (~140 m) with shales, cherts and carbonates, a middle unit with tuffaceous litharenites and upper unit of volcanoclastic sediments and ignimbrites (with zircon U-Pb ages of 543 and 546 Ma) (Bowring et al. 2007).

Cadomian rocks are not exposed in SE Zagros and the Persian Gulf region but salt diapirs are abundant. Therefore, salt diapirs can provide valuable information about the lithology, composition and age of deeply buried basal sediments and underlying basement. This paper reports results of a first study of xenoliths in the Chah-Banu salt diapir, which is the largest diapir from Larestan in the SE ZFTB. The extrusion age of SE Zagros salt diapirs seems to be Middle Miocene, as evidenced by deformation of Middle Miocene sediments (Kent 1958, 1979; Jahani et al. 2007), shortly after Arabia began to subduct beneath Iran. This extrusion time is consistent with the extrusion time of salt diapirs from SE parts of Persian Gulf (Thomas et al. 2015). We report, for the first time, the petrology, age, and isotopic composition of the exotic igneous blocks from the Chah-Banu salt diapirs. We then discuss their geochemical and isotopic signatures and show how the Cadomian crust sampled by the salt is remarkably similar to that of Oman. Then, we discuss the implications of these results for models describing the dispersion and amalgamation of Gondwana-derived Cadomian continental fragments in Iran.

2. Geological background

2-1. Regional geology

The Zagros Orogen is caused by convergence of Arabia under Iran. It can be traced along the Iraq - Iran border SE into Iran where it transitions into the Makran accretionary complex (Alavi 2007; Mouthereau et al. 2012). The Zagros Orogen comprises five parallel tectonic units from the southwest to northeast: the ZFTB (basically the accretionary prism of the Iran convergent margin), outer belt ophiolites (Kermanshah-Haji-Abad), Sanandaj-Sirjan Zone, inner belt ophiolites (Nain-Baft) and Urumieh-Dokhtar Magmatic Belt (UDMB). ZFTB contain abundant hydrocarbon reservoirs which are mainly associated with salt structures. The salt diapirs rise through the ZFTB from a thick-pile of deeply buried Ediacaran-Cambrian evaporites of the Hormuz series, which is interpreted as a stratigraphic equivalent of the Rizu-Desu series in Central Iran, the Kalshaneh Formation of E Iran and the Soltanieh Formation in central and N Iran (Stocklin 1968). Hormuz series displays a concentric structure in southern Iran and consists mainly of older multicolored (mélange-like) salts with dark dolomites and thin layers of sandstones, siltstones, cherts and marls with local yellow-brown ortho-quartzites (Stocklin 1968; Talbot & Alavi 1996). Younger gray-colored anhydritic salts and trilobite-bearing red beds with mid- Cambrian ages are also mixed with and/or overlie the older strata. These units are associated with mega-xenoliths of few hundred meters of Cambrian carbonates and red sandstone-siltstones (Husseini & Husseini 1990; Edgell 1991; Talbot et al. 2009a; Talbot et al. 2009b).

Many authors previously studied the exotic blocks from the salt diapirs of SE Zagros (for details see (Husseini & Husseini 1990)). For example, (Alavi 2004) reported U-Pb zircon age of 547±6 Ma for leucogranitic blocks in the Jahani salt diapir from SE Zagros. (Thomas et al. 2015) obtained zircons ages of 560-545 Ma for exotic blocks in the salt domes of UAE and Oman, S of the Persian Gulf. They suggested that the deposition of evaporites and terrigenous sediments along with magmatism occurred in a continental extensional setting- in a subsiding rear-arc basin- along the Gondwana margin in Late Neoproterozoic-Early Cambrian (Cadomian) time, perhaps in a continental back arc basin. Sedimentation is believed to have occurred in the Ediacaran-Lower Cambrian boundary which lies within the lower parts of the Ara group of Oman (Bowring et al. 2007). Rhyolites from Hormoz Island (Persian Gulf) show zircon U-Pb ages of 558±7 Ma and are suggested to be linked with an active continental margin (Faramarzi et al. 2015). These rhyolites are similar to volcanic rocks of the Fara Formation of Oman which yielded zircon U-Pb ages of 542 to 547 Ma (Bowring et al. 2007). There is some consensus about the formation of these salt basins and diapirs. Some believe that the Hormuz evaporate series basins formed in a volcanic rift during Lower Cambrian (e.g., (Taghipour et al. 2013)) but others argue for an arc-related basin (e.g., (Faramarzi et al. 2015)). Some of the salt domes- such as the Hormoz salt dome- are important for the exploration of the banded iron-salt formation deposits. The occurrence of these deposits is suggested to be linked with the submarine alkaline felsic magmatism within the continental rift zones (Atapour & Aftabi 2017b). Ascent of salt diapirs from Hormuz series salt deposits transported many exotic blocks of igneous, pyroclastic, sedimentary, and low-grade metamorphic rocks to the surface as mega-xenoliths. There are various volcanic lithotypes including dacites, rhyolites, trachytes, dolerites and basaltic rocks. Pyroclastic rocks are more common than lavas, and sedimentary rocks are the most abundant of all lithologies. Paleozoic strata are rarely found as xenoliths.

2-2. Samples descriptions

The Chah-Banu salt diapir in SE Zagros is oval-shaped, covers an area of ~100 km^2 and is one of the largest salt diapirs in S Iran (Fig. 1C). The Chah-Banu salt diapir is characterized by a concentric structure with salt in the core, grading outward to gypsum, and ultimately to anhydrite on the outer margins. This diapir is capped by the Lower Miocene Gachsaran (Gs) Formation and Guri member (Grm) of the Mishan Formation (Fig. 2A). The Gachsaran Formation is a succession of marls, gypsum and limestones. The Mishan Formation consists of a succession of shallow marine deposits, gray marls and thin bedded limestones, indicating that the salt dome was exposed at sea-level 15 to 20 million years ago.

The Chah-Banu salt diapir contains exotic blocks of igneous and sedimentary rocks including red sandstones, black and white dolomites, cherts, volcanoclastic and volcanic-subvolcanic rocks (rhyolites, dacites, dolerites and basalts) and minor plutonic rocks (mostly gabbroic rocks) (Fig. 2).

Exotic clasts range in size from microscopic to large kilometer-scale mega-clasts. Sedimentary structures and stratigraphic contacts between rock units are preserved in mega-clasts (Figs. 2D-F). These clasts are embedded in the Ediacaran-Early Cambrian evaporites (Figs. 2B-C and E). The contacts between Hormuz salt sediments and exotic blocks can be sharp or tectonized. In most cases exotic blocks are mixed into the evaporite matrix and look a colored mélange. Dacites show aphyric to porphyritic textures. They contain quartz, sanidine and plagioclase phenocrysts set in a microcrystalline to cryptocrystalline groundmass consisting of quartz and intergrowths of sodic plagioclase and K-feldspar (Fig. 3A). Biotite, titanite and iron oxides occur as accessory minerals. Quartz crystals with resorbed texture are the main phenocrysts (~47%). Plagioclase is altered into epidote and calcite whereas alkali feldspars show alteration into sericite. Apatite, biotite and magnetite are accessory minerals while calcite, sericite, titanite, hematite and chlorite are common secondary minerals.

Rhyolites are less abundant than dacites and occur as lava flows. These rocks have porphyritic textures and contain phenocrysts of plagioclase (5-10 %), biotite (5-7%), sanidine (~5%), and quartz (20%) set in a matrix composed mainly of glass, quartz, and sanidine microlites. Plagioclase is present as randomly oriented, tabular crystals and shows alteration to kaolinite and sericite. Coarse-grained plagioclase in some rhyolitic lavas is characterized by disequilibrium dusty and/or sieve textures, which are an indicator of rapid decompression during the eruption of magmas and/or signify magma mixing (Nelson & Montana 1992).

Dolerites are nearly holocrystalline with altered clinopyroxenes, saussuritized plagioclase and chloritic groundmass (Fig. 3B). Basalts are generally fine-grained with holocrystalline to porphyritic and intergranular textures. The main constituents of these rocks are plagioclase laths and altered clinopyroxenes (Fig. 3C), whereas the accessory minerals consist of titanomagnetite and apatite. Epidote, chlorite, calcite and albite are common secondary minerals. Some basalts contain altered plagioclase laths surrounded by altered glasses representing intersertal texture (Fig. 3D).

Gabbros have plagioclase (50-60 wt. %), amphibole (20-30 wt. %) and clinopyroxene (5-10 wt. %) as primary constituents (Fig. 3E), although minor olivine, orthopyroxene, and biotite can be observed in some samples (Figs. 3E-F). Epidote, clinozoisite and chlorite are secondary minerals. These rocks are generally medium grained with a granular texture. Clinopyroxenes are altered into amphiboles, whereas plagioclase shows alteration into zoisite and albite. Volcanoclastic rocks contain altered minerals (as pseudomorph into calcite and/or chlorite) and rock fragments set in a groundmass containing fine-grained to cryptocrystalline quartz and chlorite (Figs. 3G-H).

3. Analytical procedures

Only a brief synopsis of procedures is given here; see Appendix A for details. Twenty igneous rocks from exotic blocks were analyzed using XRF method at the Australian ALS lab (Table 1). Concentrations of trace elements were determined by Inductively Coupled Plasma Mass Spectroscopy

(ICP-MS) using a Thermo Scientific X-Series 2 in the Department of Earth Sciences at the University of Durham, following a standard nitric and hydrofluoric acid digestion (Ottley et al. 2003). The bulk rock trace elements analyses for exotic blocks are shown in Table 2. Sr and Nd isotopic composition of igneous rocks were analyzed at Laboratório de Geologia Isotópica da Universidade de Aveiro, Portugal. Initial values of the Nd isotope of samples were calculated according to the procedure of (Depaolo 1981). Bulk rock Sr-Nd isotopic data are presented in Table 3. Zircon U-Pb dating used LA-ICPMS at Geochemical Analysis Unit (GAU), CCFS/GEMOC, Macquarie University. LA-ICPMS U-Pb zircon analytical data is summarized in Table 4. *In situ* zircon Lu-Hf isotopic analyses were performed using a Nu Plasma multi-collector ICP-MS, coupled to a Photon Machines 193 nm ArF excimer laser system at CCFS (Macquarie University). Zircon Hf isotope data are presented in Table 5.

4. Results

4-1. Zircon U-Pb Geochronology

We analyzed zircon U-Pb ages for two samples of exotic clasts including gabbro and dacite. These results are discussed below.

Dacite

Zircons in dacite sample C-7 have a wide variation of U (86-3958 ppm) and Th (44-1400 ppm) contents and their Th/U ratios vary from 0.4 to 3.9. Twenty-five analyses from this sample yielded a mean age of 538.2±2.2 Ma (MSWD=0.8) (Fig. 4A) which is interpreted as the crystallization age of dacite sample C7. One analyzed spot on a zircon core show $^{206}Pb/^{238}U$ age of 1762 ± 52 Ma.

Gabbro

We analyzed gabbro sample C21 for zircon U-Pb ages (Table S1). U, and Th contents range from 289 to 2169 ppm and 516 to 10409 ppm, respectively. The Th/U ratio varies from 1.7 to 3.5, except one point with Th/U =6.9, which is typical for zircons from mafic igneous rocks (Belousova et al. 2002). Twenty-five analyzed zircons yielded a mean age of 539.0±1.8 Ma (MSWD=0.8) (Fig. 4B).

4-2. Geochemistry of igneous rocks

Major, trace and rare earth element contents of exotic magmatic rocks from the Chah-Banu salt diapir are given in Tables 1 and 2. There are significant compositional variations among the analyzed samples for some major elements; some of this variability is due to alteration. The effect of alteration is shown by variable LOI contents of these samples, which varies widely from 1.2-8.8 *wt* %. SiO_2 content varies from 40 to 75 *wt* %. Chah-Banu Cadomian intrusive and sub-volcanic rocks can be subdivided into gabbros and dolerites; whereas volcanic rock have basaltic to dacitic- rhyolitic compositions. Because Chah-Banu igneous rocks interacted with Na-rich salt, we use immobile trace elements for classifying them.

Based on Nb/Y *vs* Zr/TiO_2 diagram (Hastie et al. 2007), the Chah-Banu rocks are subdivided into mafic and felsic rocks; mafic rocks (including gabbros, basalts and dolerites) have basaltic composition while felsic rocks show dacite-rhyolite composition (Fig. 5A). This bimodal composition is similar to that of igneous rock clasts from Oman salt domes (Fig. 5A). The Chah-Banu gabbros contain 48-49.2 *wt* % SiO_2 with wide variations of K_2O (1.5-2 *wt*%) and Na_2O (2.4-4.2 *wt* %) contents. Basalts have similar SiO_2 (44.2-47.4 *wt* %), MgO (6.3-11.4 *wt*%) and Al_2O_3 (13.6-15.8 *wt* %) contents; alkali contents vary widely: K_2O (0.2-6.1 *wt* %) and Na_2O (0.1-3.8 *wt*%). Dolerites have broadly similar SiO_2 (45.7-48.6 *wt* %), MgO (5.9-9 *wt*%) and Al_2O_3 (13.3-16.7 *wt* %) contents; alkali contents vary widely: K_2O (3.1-6 *wt* %) and Na_2O (0.6-2 *wt*%). Dacites and rhyolites are characterized by wide variation of SiO_2 (65.1-75.9 *wt* %), K_2O (0.9-3.4 *wt* %) and Na_2O (2.2-6.2 *wt* %). Based on the Co *vs* Th diagram (Fig. 5B), mafic rocks classify as low- to medium-K calc-alkaline series whereas dacites and rhyolites plot in high K calc-alkaline-shoshonitic series.

Chondrite-normalized rare earth element (REE) patterns of gabbros, basalts and dolerites (Fig. 6A) show nearly flat to slightly enrichment in light rare earth elements (LREEs) with $La_{(n)}/Yb_{(n)}$ ratio of 1.17 to 3.15, without conspicuous Eu negative anomalies (Eu/Eu*= 0.65 to 1.03). On a multi-element, N-MORB- normalized diagram (Figs. 6B), these rocks exhibit positive anomalies for Rb, Ba, U, K, Pb and with negligible negative anomalies in Nb relative to primitive mantle. Basalts, dolerites and gabbros show relatively smooth, OIB-like trace element patterns with no strong HFSE depletions.

Chondrite-normalized REE profiles of dacites-rhyolites (Fig. 6C) show moderately variable $La_{(n)}/Yb_{(n)}$ ratio of 0.99-7.32, with conspicuous negative Eu anomalies (Eu/Eu*= 0.16 to 0.23). On a multi-element, N-MORB- normalized diagram (Figs. 6D), these rocks exhibit positive anomalies for Rb, Ba, U, K, Pb and with negative anomalies in Ti, P and Nb relative to LREEs. The geochemical signatures of dacites-rhyolites, including depletion in Nb, Ti and enrichment in large-ion lithophile elements (LILEs) and high ratios of LREEs/HREEs, are similar to the geochemical characteristics of continental arc magmatic rocks (Ducea et al. 2010).

4-3. Bulk rock Sr-Nd and zircon Hf isotopes

We analyzed 9 samples (5 mafic and 4 felsic rocks) of Chah-Banu exotic clasts for Sr-Nd isotopes (Table 3). Initial $^{87}Sr/^{86}Sr_{(i)}$ and $^{143}Nd/^{144}Nd_{(i)}$ of these rocks is re-calculated based on zircon U-Pb ages. These rocks show initial εNd(t) values of +4.7 to +6.8 for mafic rocks and -3.4 to -4.1 for the felsic rocks (Fig. 7). Mafic rocks have depleted mantle model ages (T_{DM}) of ~ 0.8-1.7 Ga, while dacites have mostly older T_{DM} of ~1.5-2.1 Ga. $^{87}Sr/^{86}Sr_{(i)}$ values show considerable variations for mafic (0.7059 to 0.7085) and felsic rocks (0.7081 to 0.7091), which might partially reflect alteration. Zircons from dacite sample C-7 have negative εHf(t) values of –1.1 to –8.3 (*av* –3.4), suggesting that nearly all zircons from dacites have enriched radiogenic signatures with significant contribution of crustal components in the melt source or during the melt ascent and emplacement. Crustal model ages

(T_{DM}^{C}) of zircons from dacites are in the range of 1.6 to 2 Ga. Zircons from gabbro sample C-21 have variable εHf(t) values of +4.5 to +8.5, indicating that mantle-derived juvenile magmas were responsible for gabbroic clasts. Crustal model ages of zircons from gabbro sample C-21 are in the range of 1 to 1.2 Ga.

The significantly less radiogenic Nd and zircon Hf isotope signature of felsic rocks compared with mafic rocks shows that even though mafic and felsic magmas were produced about the same time, they were derived from different magma sources.

5. Discussion

Cadomian magmatic rocks constitute the main rock units that formed on the northern margin of Gondwana in a >5000 km long belt in Eastern N. America, Europe (Avigad et al. 2016), as well as Turkey, Iran and Tibet (Wang et al. 2016). Our new data confirm that although Cadomian igneous rocks constitute the main substrate of Iran north of the Main Zagros Thrust, there is also Cadomian crust beneath at least some of the Zagros Fold and Thrust Belt. We do not know if the exotic blocks within the salt diapirs from SE Iran come from subducted Arabia crust or represents a southern extension of Iranian basement, although we prefer the first interpretation. Xenoliths from more salt diapirs from SE Iran and N Arabia should be studied and compared in order to address this question. Below, we discuss the origin and petrogenesis of Cadomian exotic clasts from the Chah-Banu salt diapir, compare the composition of exotic blocks with in-situ Cadomian rocks of Iran, explore the geodynamic implications of our results, and address the relation of Cadomian igneous activity to deposition of the Hormuz Salt.

5-1. Petrogenesis of igneous exotic blocks

Chah-Banu exotic mafic and felsic magmatic rocks that formed about 538-539 Ma, but they are not comagmatic. Mafic rocks are OIB-like mantle melts and felsic rocks are arc-like and generated from remelting Paleoproterozoic continental crust.

Chah- Banu mafic igneous rocks- including gabbros, dolerites and basalts- are enriched in LREEs, Rb, Ba, Th, U, Pb and K, without strong depletion in Nb, Ta, and Ti (Fig. 6A-B). These are features of intraplate magmas and those erupted in rift zones; they are also found in continental back-arc regions. The Chah-Banu mafic rocks plot in both volcanic-arc and within-plate fields in Rb *vs* Y+Nb, Rb *vs* Ta+Yb, Nb *vs* Y and Ta *vs* Yb plots (Fig. 9). Mafic rocks show geochemical similarities to E-MORBs in the Th/Yb *vs* Ta/Yb (Fig. 10A) (Tindle & Pearce 1983). In the Nb/U *vs* Nb plot, these rocks are similar to MORBs and OIBs (Fig. 10C) whereas in the Ce/Nb *vs* Y/Nb gabbros, dolerites and basalts are similar to IAB (Fig. 10D). These rocks have different $La/Yb_{(N)}$ ratios (Fig. 10B) and probably reflect different magmatic sources (enriched with high $La/Yb_{(N)}$ *vs* quite depleted with low $La/Yb_{(N)}$ ratios). These rocks are characterized by positive bulk rock εNd(t) (+4.7 to +6.8) and zircon εHf(t) values (+4.5 to +8.5), showing a juvenile mantle source.

HFSE concentrations and N-MORB-normalized patterns of gabbros, dolerites and basalts are similar to those of E-MORBs and OIBs (Fig. 6B), although they have more LILE content. Their high HFSE concentrations suggest generations from an enriched mantle source. Enriched mantle sources similar to EM-I and EM-II can generate enriched magmas with negative εNd(t) values (Zindler & Hart 1986), which is not the case for Chah-Banu gabbros, dolerites and basalts. We believe the positive εNd(t) and εHf(t) values in these rocks, along with their enrichment in K, Rb, REEs and other HFSEs suggest a metasomatized mantle source such as sub-continental lithospheric mantle (SCLM). Such compositions are is consistent with formation in a continental rift and/or continental back-arc regions.

In contrast to the mafic rocks, most felsic rocks show affinities with arc magmas. These have I-type geochemical characteristics in Na_2O+K_2O, K_2O/MgO, Zr and Nb *vs* 10000×Ga/Al discrimination diagrams of (Whalen et al. 1987), except for sample C-17 which shows tendency to A-type granites (Fig. 8). Felsic rocks also fall in the VAG field in Rb *vs* Y+Nb, Rb *vs* Ta+Yb, Nb *vs* Y and Ta *vs* Yb plots (Fig. 9). Dacites-rhyolites show geochemical similarities to continental magmatic arc-related rocks in the Th/Yb *vs* Ta/Yb (Fig. 10A) (Tindle & Pearce 1983). The Th/Ta ratio of dacites-rhyolites changes from 27.5 to 17.7 and are similar to magmatic rocks from active continental margins (Fig. 10B). In the Ce/Nb *vs* Y/Nb and Nb/U *vs* Nb plots, dacites-rhyolites are most like island-arc basalts (IAB) (Figs. 10C-D). Dacites-rhyolites belong to the high-K calc-alkaline/shoshonitic magmatic series and share their geochemical signatures in terms of trace elements (Figs. 6C-D) and Sr-Nd isotopes (Fig. 7). These rocks are cogenetic and may have formed from a similar source.

Dacites-rhyolites from Chah-Banu salt diapirs are enriched in LREEs, Rb, Ba, Th, U, Pb and K, and depleted in Nb, Ti, features of active continental arc magmas (Pearce & Peate 1995b; Baier et al. 2008). The flat MREE to HREE patterns for dacites-rhyolites suggest that garnet was absent in their sources during partial melting. Such felsic magmas may have formed by partial melting of older continental crust and/or due to interaction of mantle melts with older crust. The peraluminous composition of these rocks also supports a crustal component in the genesis of these rocks, probably via crustal melting and fractional crystallization (Rudnick 1992, 1995). Chah-Banu dacites-rhyolites have high concentrations of Th (high Th/Yb ratios of 2.4-5.0) with high initial $^{87}Sr/^{86}Sr$ ratios and negative εNd(t) (–3.45 to – 4.05) and εHf(t) values (–1.1 to –8.3), confirming the importance of older continental crust during magma genesis and evolution. Nd-isotope crustal residence ages (T_{DM}) of dacites-rhyolites range from 1.5 to 2.1 Ga, suggesting that Mesoproterozoic or older crust was involved in their genesis. Furthermore, the negative Eu anomaly indicates that these melts experienced low pressure plagioclase fractionation in crustal magma chambers.

It is generally believed that I-type felsic rocks may be derived by mixing of mantle-derived magmas with crustal melts and/or contamination of mantle melts with crustal components via assimilation-fractional crystallization (AFC) (e.g., (Hildreth et al. 1991; Huang et al. 2013)). We propose that the unradiogenic bulk rock εNd(t) (−7.7 to −6.2) and zircon εHf(*t*) ((–1.1 to –8.3) isotopic values for felsic igneous clasts indicates that these felsic magmas may have formed by partial melting of older continental crust and/or via interaction of mantle melts with such crust via AFC. The presence of xenocrystic zircons (with ages of 1.7 Ga) also supports this idea.

5-2. Comparison of exotic blocks with exposed Cadomian basement of Iran

An important question concerning the evolution and genesis of the exotic magmatic blocks is how are these related to similar age igneous rocks that outcrop in Iran and that are documented from the subsurface of NE Arabia, UAE, and Oman? The Cadomian magmatic episode in Iran occurred above a S-dipping subduction zone beneath northern Gondwana (Moghadam et al. 2017b). This was accompanied by widespread igneous activity, best known from Iran-Anatolian Cadomian arcs. Cadomian magmatism in Iran lasted from 600 Ma to 500 Ma (Moghadam et al. 2017c; Moghadam et al. 2017b) but was especially intense during a flare-up at 570 to 525 Ma (Moghadam et al. 2017a; Shafaii Moghadam et al. 2020). Chah-Banu igneous xenoliths formed during this flare-up, which is thought to reflect strong extension in the convergent margin. (Moghadam et al. 2017a; Shafaii Moghadam et al. 2020) suggest that slab steepening, perhaps accompanied by delamination or slab roll-back at the northern Gondwana convergent margin caused this extension and flare-up in Iran-Anatolia.

Cadomian magmatism differed in various parts of Iran. Cadomian magmatic rocks from NE Iran include: a) calc-alkaline gabbros and diorites with zircon U-Pb ages of ∼530 to 556 Ma; b) I-type granitic intrusions with ages of ∼532-552 Ma; c) calc-alkaline felsic volcanic rocks with U-Pb zircon age of ∼550 Ma; d) minor alkaline (OIB-like) mafic rocks with zircon U-Pb ages of ~545 to 555 Ma; and e) psammitic to volcanogenic metasediments with detrital age peaks at ∼549-552 Ma (Moghadam et al. 2020). Cadomian calc-alkaline magmatic rocks from NE Iran are isotopically variable, with bulk rock εNd(t) of −6 to +7, zircon εHf(t) of −9.6 to +10.7 and zircon $\delta^{18}O$ values of ∼+5 to > +9. These isotopic data suggest the involvement of both juvenile melts and older continental crust. In contrast, alkaline mafic rocks are characterized by strong enriched-mantle signatures (high Nb/Yb ratio, without Nb-Ta depletion). The generation of these alkaline magmas is attributed to the involvement of enriched mantle (Balaghi et al. 2010; Veiskarami et al. 2019).

Cadomian rocks from NW Iran are typically composed of I-type granitic to tonalitic gneisses, granitoids, migmatites, granulites, grading upward into felsic volcanic rocks with zircon U-Pb ages of ∼620 to 500 Ma (Hassanzadeh et al. 2008; Moghadam et al. 2017c; Moghadam et al. 2017b; Moghadam et al. 2019). These magmatic rocks are characterized by medium to high-K calc-alkaline signatures, with low εHf(t) values of -7 to -0.7, signifying significant involvement Paleo-Proterozoic to Archean continental crust.

Cadomian rocks from central Iran include I- and A-type granites, ortho- and para-gneiss, amphibolites, pelitic schists with zircon U-Pb ages of 547 to 525 Ma (Ramezani & Tucker 2003). A-type granites have juvenile isotopic signatures, with εNd(t) and εHf(t) values of +0.3 to +4.0 and +1.1

to +5.1, respectively. The generation of these granites requires the involvement of a melt with moderately radiogenic Nd-Hf isotopic compositions, probably from fractionation of a mafic partial melt of moderately enriched mantle. I-type granites from central Iran have negative bulk rock εNd(*t*) (-6.2 to -7.7) and variable zircon εHf(*t*) (-6.6 to +6.3), showing significant influences of crustal components during magma genesis and evolution. Alkaline rhyolites are also reported from central Iran (Momenzadeh & Heidari 1995). In addition, Cadomian A-type granites have been described from the Sanandaj-Sirjan Zone of Iran (Shakerardakani et al. 2015; Shabanian et al. 2018). These intrusive rocks have zircon U-Pb ages of 568 ±11 Ma (Shakerardakani et al. 2015) and 525.6 ±4 Ma (Shabanian et al. 2018) and show crustal Nd isotope signatures with εNd(t)= –1.2 to –1.5. In summary it seems that there are both calc-alkaline I-type granitoids and within-plate A-type granites and alkaline mafic rocks in Cadomian exposures of Iran (Figs. 8-10).

Cadomian exotic blocks from SE Iran are compositionally bimodal and include both felsic, calc-alkaline rocks and mafic, E-MORB-like or geochemically-isotopically enriched rocks. Enriched (OIB-like) igneous rocks are rare in the Cadomian basement of Iran. The generation of these OIB-like magmas requires an enriched mantle. OIB-like mafic rocks such as exotic clasts from SE Iran or mafic rocks from central Iran are also accompanied by felsic rocks, showing a bimodal magmatic episode. Two different magma sources can be considered for these rocks; the generation of the OIB-like magmas requires the involvement of enriched mantle, but I-type felsic rocks require involvement of old continental crust.

5-3. Geodynamic implications

The main result of our studies is discovery of Cadomian bimodal exotic clasts in the Chah-Banu salt diapir. OIB-like mafic rocks and calc-alkaline felsic rocks are the same age but have different sources. There are several scenarios suggested for the genesis of the coeval felsic and OIB-like mafic rocks in central Iran and/or in Hormuz series including; 1- Formation in an intra-plate rift setting (Momenzadeh & Heidari 1995); 2- Formation above a subduction zone (Ramezani & Tucker 2003); 3- Submarine volcanism in an extensional back-arc basin (Faramarzi et al. 2015); 4- Generation in fault-bounded trough basins during Gondwana rifting (Berberian & King 1981; Talbot et al. 2009a); and 5- Formation in a continental, intra-plate rift (Atapour & Aftabi 2017a; Atapour & Aftabi 2017b). Thick sequences of terrigenous rocks such as sandstones with evaporites (halites, potash salts, anhydrites and gypsum) and banded iron-salt deposits in close association with bimodal magmatic rocks in Hormuz series demonstrate the magmatic rocks formed in a rifted basin.

The presence of OIB-like rocks is important as these indicate a continental rift, but the presence of calc-alkaline and subduction-related rocks also implicates a convergent margin for the formation of these rocks. These two types of igneous rocks with different geochemical and isotopic signatures formed simultaneously in a single tectonic setting.

Extensional rifts are often found in back-arc regions of active continental margins and many of these are related to slab roll-back and ocean-ward retreating of the subduction hinge (Ducea et al. 2017). Slab rollback is important because this causes upper plate extension, crustal thinning, continental rifting and juvenile crustal addition (Miskovic & Schaltegger 2009). In the case of the Cadomian convergent margin of Iran, extension and crustal thinning may have led to decompression melting of SCLM beneath the rear-arc. Low degree of melting of enriched SCLM and/or plume-influenced sub-arc mantle can the generate OIB-like melts we document. Such melts may be difficult to distinguish from OIB from oceanic Islands and/or continental plumes which are sometimes more undersaturated and isotopically evolved. Flux melting in the sub-arc mantle beneath the retro-arc crust may also have generated mafic melts that can interact with overlying continental crust to produce I-type felsic rocks via assimilation and fractional crystallization.

5-4. Relation of Cadomian igneous activity to Hormuz Salts

Finally, what does our study reveal about the age of the Hormuz salt in Iran? This is broadly interpreted to have formed ~550 Ma (Talbot & Alavi 1996) but tighter age constraints are lacking. Regional considerations are useful because the Hormuz Salt and its equivalents are found in a very large region that extends south to Arabia and Oman and east into Pakistan. Formation of evaporites in Iran- i.e., the Hormuz series- and its equivalent in southern Oman (the Ara Formation), central Iran (the Ravar Formation) and N Pakistan (the ~555-538 Ma Salt Range Formation; (Hughes et al. 2019)) are suggested to have been deposited in retro-arc basins (Husseini & Husseini 1990; Edgell 1991; Bowring et al. 2007; Talbot et al. 2009a; Talbot et al. 2009b).

We cannot be sure that these salt deposits formed at the same time over this huge area, but they might be correlative. In SE parts of the Persian Gulf, (Thomas et al. 2015) suggested that salt was deposited ~540-500 Ma. The best age constraints come from Oman, where (Bowring et al. 2007) studied the Ara Group in the South Oman Salt Basin where evaporites are interbedded with ash beds dated at about 547, 542, and 541 Ma, slightly older than the 538-539 Ma ages we report. The presence of ash beds in the Ara Group suggests that some igneous activity happened at the same time as salt deposition. What was the relationship between Hormuz salt deposition and the 538-539 Ma igneous rocks we studied? They could be slightly older than the salt, slightly younger, or the same age. If igneous rocks are older, they must be plucked from beneath and somehow incorporated in the rising salt diapir. It is easier to imagine that blocks of volcanic rocks that flowed over the salt were incorporated into the rising diapir. Easiest of all is if lava flowed into salt and was buried by salt. In this case irregular margins of igneous bodies with chilled margins are expected. The occurrence of banded jaspilitic hematite and salt minerals as rhythmic layering and its association with rhyolites and rhyolitic tuffs (without contact metamorphism) suggests that the submarine magmatism was associated with iron and salt deposition (Atapour & Aftabi 2017b).

6. Conclusions

Our new zircon U-Pb ages as well as geochemical and isotopic data from Cadomian magmatic rock clasts of SE Zagros salt domes allow us to distinguish two types of rocks; felsic volcanic rocks with calc-alkaline and I-type geochemical signatures and mafic volcanic and plutonic rocks with OIB-like geochemical characteristics. Zircon U-Pb ages show that both rock types formed simultaneously at 539 to 538 Ma. Trace element geochemistry, bulk-rock Sr-Nd and zircon Hf-isotope composition indicate involvement of both mantle melts and an older continental crust and/or re-melting of an old continental during the generation of Cadomian felsic rocks, whereas an enriched mantle such as SCLM was responsible for the genesis of mafic rocks. We propose that a rifted retro-arc basin formed behind the Cadomian magmatic arc and was responsible for magmatism and deposition of evaporites, terrigenous sediments and iron-salt deposits. The formation of this basin was caused by crustal stretching due to the trench roll-back as a result of subduction of Prototethyan ocean beneath N Gondwana.

7. Acknowledgments

This study used instrumentation funded by ARC LIEF and DEST Systemic Infrastructure Grants, Macquarie University, NCRIS AuScope and Industry. This is contribution XXX from the ARC Centre of Excellence for Core to Crust Fluid Systems (http://www.ccfs.mq.edu.au) and XXX in the GEMOC Key Centre (http://www.gemoc.mq.edu.au). This is UTD geosciences contribution # 13xx. We acknowledge support from Foundation for Science and Technology of Portugal, through project UID/GEO/04035/2019 (Geobiotec).

8. Figure captions

Figure 1- A- Simplified geological map of Iran showing distribution of Cadomian magmatic rocks, Cadomian salt-domes, Late Cretaceous ophiolites and Cenozoic magmatic rocks. B- Simplified geological map showing location of Persian Gulf and Oman salt-basins. C- Simplified geological map of the Chah-Banu salt dome.

Figure 2- A- Stratigraphical contact between Chah-Banu salt diapir and Early Miocene Gachsaran Formation (Gs) and Middle Miocene Guri member (Grm) of the Mishan Formation. B- Igneous blocks between salts and gypsum-anhydrites. C- Mélange-like appearance of Chah-Banu salt-dome including blocks of red sandstones, dark green magmatic rocks, and black dolomites in a matrix of salt and gypsum-anhydrite. D- Contact between dolomite exotic block and cherts. E- Alteration of red sandstones, dark green magmatic rocks, cherts and dolomites. F- Large block of black dolomite.

Figure 3- Microphotographs of magmatic rocks from the Chah-Banu salt dome. A- Rare altered sanidine phenocryst set in a microcrystalline to cryptocrystalline groundmass consisting of quartz and

intergrowths of sodic plagioclase and K-feldspar in rhyolite. B- Altered clinopyroxenes, saussuritized plagioclase and chloritic groundmass in dolerite. C and D- Holocrystalline to intersertal textures in basalt with plagioclase laths and altered clinopyroxenes. E and F- Plagioclase, amphibole, olivine and orthopyroxene in gabbro. G and H- The presence of altered minerals (as pseudomorphed into calcite and/or chlorite) and rock fragments set in a groundmass containing fine-grained to cryptocrystalline quartz and chlorite in volcanoclastic rocks.

Figure 4- Concordia and weighted mean $^{206}Pb/^{238}U$ age plots for the investigated zircons from the Cadomian exotic blocks from Chah-Banu salt diapir.

Figure 5- Zr/TiO_2 *vs* Nb/Y (A) and Th *vs* Co (B) plots for the classification of magmatic clasts from Chah-Banu salt-dome. Data for Cadomian alkaline rocks are from (Balaghi et al. 2010; Shabanian et al. 2018; Maleki et al. 2019; Veiskarami et al. 2019), whereas data for Cadomian calc-alkaline rocks come from (Badr et al. 2013; Balaghi et al. 2014; Moghadam et al. 2015; Moghadam et al. 2016; Moghadam et al. 2017c; Shafaii Moghadam et al. 2020). Data for Hormoz salt domes is from (Faramarzi et al. 2015), whereas data for salt domes of UAE and Oman come from (Thomas et al. 2015).

Figure 6- Chondrite-normalized rare earth element (A and C) and N-MORB-normalized trace element patterns (B and D) for the magmatic clasts from Chah-Banu salt dome. Chondrite and N-MORB normalized values are taken from (Sun & McDonough 1989). The composition of OIB and E-MORB is also shown for comparison.

Figure 7- Initial epsilon Nd *vs* $^{87}Sr/^{86}Sr$ plot for the magmatic blocks from Chah-Banu salt-dome. Bulk rock Sr-Nd isotope data for Cadomian rocks of Iran and Anatolia are from (Ustaomer et al. 2009; Gursu et al. 2015; Moghadam et al. 2015; Moghadam et al. 2016; Moghadam et al. 2017a; Honarmand et al. 2018; Daneshvar et al. 2019; Shafaii Moghadam et al. 2020; Sepidbar et al. revised).

Figure 8- K_2O+Na_2O, K_2O/MgO, Zr and Nb *vs* 10000Ga/Al plots (Whalen et al. 1987) for classification of magmatic blocks from Chah-Banu salt-dome. Data for Cadomian alkaline rocks are from (Balaghi et al. 2010; Shabanian et al. 2018; Maleki et al. 2019; Veiskarami et al. 2019), whereas data for Cadomian calc-alkaline rocks come from (Badr et al. 2013; Balaghi et al. 2014; Moghadam et al. 2015; Moghadam et al. 2016; Moghadam et al. 2017c; Shafaii Moghadam et al. 2020). Data for Hormoz salt domes is from (Faramarzi et al. 2015), whereas data for salt domes of UAE and Oman come from (Thomas et al. 2015).

Figure 9- A- Rb *vs* Y+Nb, B- Rb *vs* Yb+Ta, C-Nb *vs* Y and D- Ta *vs* Yb diagrams (Pearce et al. 1984) for classification of magmatic blocks from Chah-Banu salt-dome. Data for Cadomian alkaline rocks are from (Balaghi et al. 2010; Shabanian et al. 2018; Maleki et al. 2019; Veiskarami et al. 2019), whereas data for Cadomian calc-alkaline rocks come from (Badr et al. 2013; Balaghi et al. 2014; Moghadam et al. 2015; Moghadam et al. 2016; Moghadam et al. 2017c; Shafaii Moghadam et al. 2020). Data for Hormoz salt domes is from (Faramarzi et al. 2015), whereas data for salt domes of UAE and Oman come from (Thomas et al. 2015).

Figure 10- A- Th/Yb *vs* Ta/Yb (Pearce & Peate 1995a), B- La/$Yb_{(N)}$ *vs* La (Bi et al. 2016), C- Nb/U *vs* Nb (Kepezhinskas et al. 1996) and D- Ce/Nb *vs* Y/Nb (Eby 1992) plots for magmatic clasts from Chah-Banu salt-dome. MORB and OIB fields in C and D panels are after (Hofmann et al. 1986). Data for Cadomian alkaline rocks are from (Balaghi et al. 2010; Shabanian et al. 2018; Maleki et al. 2019; Veiskarami et al. 2019), whereas data for Cadomian calc-alkaline rocks come from (Badr et al. 2013; Balaghi et al. 2014; Moghadam et al. 2015; Moghadam et al. 2016; Moghadam et al. 2017c; Shafaii Moghadam et al. 2020). Data for Hormoz salt domes is from (Faramarzi et al. 2015), whereas data for salt domes of UAE and Oman come from (Thomas et al. 2015).

9. Table captions

Table 1- Major element analysis of the exotic clasts from the salt domes of south Iran.

Table 2- Bulk rock trace and rare earth elements content of magmatic rocks from the exotic clasts of salt domes from southern Iran.

Table 3- Bulk rock Sr-Nd isotopic composition of the exotic clasts from salt domes of south Iran.

Table 4- Zircon U-Pb ages of the exotic blocks from salt domes of southern Iran.

Table 5- Zircon Lu-Hf isotope composition of the Cadomian exotic blocks from salt domes of southern Iran.

10. Appendix A

Twenty igneous rocks from exotic blocks were selected for the whole-rock geochemical analysis. Whole rock major elements were analyzed using XRF method at the Australian ALS (Table 1). Concentrations of trace elements were determined by Inductively Coupled Plasma Mass Spectroscopy (ICP-MS) using a Thermo Scientific X-Series 2 in the Department of Earth Sciences at the University of Durham, following a standard nitric and hydrofluoric acid digestion (Ottley et al. 2003). Sample preparation was undertaken in clean air laminar flow hoods. Briefly the procedure is as follows; into a Teflon vial 4ml HF and 1ml HNO_3 (SPA, ROMIL Cambridge) is added to 100 mg of powdered sample, the vial is sealed and left on a hot plate at 150 °C for 48 h. The acid mixture was evaporated to near dryness, the moist residue has 1 ml HNO_3 added and evaporated again to near dryness. 1 ml HNO_3 was again added and evaporated to near dryness. These steps convert insoluble fluoride species into soluble nitrate species. Finally, 2.5 ml HNO_3 was added and diluted to 50 ml after the addition of an internal standard giving a final concentration of 20 ppb Re and Rh. The internal standard was used to compensate for analytical drift and matrix suppression effects. Calibration of the ICP-MS was via international rock standards (BHVO-1, AGV-1, W-2, and NBS688) with the addition of an in-house standard (GP13) (Ottley et al. 2003). These standards and analytical blanks were prepared by the same techniques as for the THO samples. To improve the signal-to-noise threshold for low abundances of incompatible trace elements in ultramafic rocks, instrument dwell times were increased (Ottley et al. 2003). The composition of the reference samples (W-2, AGV-1, BHVO-1, BE-N, NBS688) was analyzed as unknowns during the same analytical runs. For the analyzed elements, reproducibility of these reference samples is generally better than 2% and the measured composition compares favorably with that published information in (Potts et al. 1992). The bulk rock trace elements analyses for exotic blocks are shown in Table 2.

Sr and Nd isotopic composition of igneous rocks has been analyzed at Laboratório de Geologia Isotópica da Universidade de Aveiro, Portugal. The selected powdered samples were dissolved with HF/HNO_3 in Teflon Parr acid digestion bombs at 200 °C. After evaporation of the final solution, the samples were dissolved with HCl (6 N) and dried down. The elements for analysis were purified using a conventional two-stage ion chromatography technique: (i) separation of Sr and REE elements in ion exchange column with AG8 50 W Bio-Rad cation exchange resin; (ii) purification of Nd from other lanthanide elements in columns with Ln resin (EiChrom Technologies) cation exchange resin. All reagents used in sample preparation were sub-boiling distilled, and pure water was produced by a Milli-Q Element (Millipore) apparatus. Sr was loaded, with H_3PO_4, on a single Ta filament, whereas Nd was loaded, with HCl, on a Ta outer-side filament in a triple filament arrangement. $^{87}Sr/^{86}Sr$ and $^{143}Nd/^{144}Nd$ isotopic ratios were determined using a Multi-Collector Thermal Ionisation Mass Spectrometer - TIMS - VG Sector 54. Data were obtained in dynamic mode with peak measurements at 1-2 V for ^{88}Sr and 0.5-1 V for ^{144}Nd. Sr and Nd isotopic ratios were corrected for mass fractionation relative to $^{88}Sr/^{86}Sr=0.1194$ and $^{146}Nd/^{144}Nd=0.7219$. During this study, the SRM-987 standard gave a mean value of $^{87}Sr/^{86}Sr= 0.710255\pm23$ (N=10; 95% c.l.) and the JNdi-1 standard yielded $^{143}Nd/^{144}Nd= 0.5121009\pm66$ (N=12; 95% c.l.). Initial values of the Nd isotope of samples were calculated according to the procedure of (Depaolo 1981). Bulk rock Sr-Nd isotopic data are presented in Table 3.

Zircon U-Pb dating has used LA-ICPMS at Geochemical Analysis Unit (GAU), CCFS/GEMOC, Macquarie University. For LA-ICPMS analysis, zircons were separated following electrostatic disaggregation (selFrag) of the rock sample, then using standard gravimetric and magnetic techniques; grains were picked under a binocular microscope and mounted in epoxy discs for analysis. All grains were imaged by CL and BSE to provide maps to guide the choice of analytical spots. Zircon U-Pb ages were obtained using a 193 nm ArF EXCIMER laser with an Agilent 7700 ICP-MS system. Detailed method descriptions is given by (Jackson et al. 2004). The ablation conditions included beam size (30 µm), pulse rate (5Hz) and energy density (7.59 J/cm^2). Analytical runs comprised 16 analyses with 12 analyses of unknowns bracketed by two analyses of a standard zircon GJ-1 at the beginning and end of each run, using the established TIMS values (^{207}Pb/^{206}Pb age= 608.5 Ma, (Jackson et al. 2004)). U-Pb ages were calculated from the raw signal data using the on-line software package GLITTER (Griffin et al. 2008). U-Pb age data were subjected to a common-lead correction, except for those with common-Pb concentrations lower than detection limits. The results were processed using the ISOPLOT program of (Ludwig 2003). The external standards, zircons 91500 and Mud Tank, gave mean ^{206}Pb/^{238}U ages of 1063.5±1.8 Ma (MSWD=1.3) and 731.1±1.2 Ma (MSWD=0.77), respectively, which are similar to the recommended ^{206}Pb/^{238}U ages of 1062.4±0.4 Ma and 731.9±3.4 Ma respectively (Woodhead & Hergt 2005; Chang et al. 2006; Yuan et al. 2008). LA-ICPMS U-Pb zircon analytical data is summarized in Table 4.

In situ zircon Lu-Hf isotopic analyses were performed using a Nu Plasma multi-collector ICP-MS, coupled to a Photon Machines 193 nm ArF excimer laser system at CCFS (Macquarie University). The analyses were carried out using the Nu Plasma time-resolved analysis software. The methods, including calibration and correction for mass bias, are described by (Griffin et al. 2000; Griffin et al. 2004). The ablation spots (55 µm) for the Hf isotope analyses were situated close to the U-Pb analysis positions on each grain. The accuracy of the Yb and Lu corrections during LA-MC-ICPMS analysis of zircon has been demonstrated by repeated analysis of standard zircons with a range in ^{176}Yb/^{177}Hf and ^{176}Lu/^{177}Hf. Four secondary standards (Mud Tank and Temora) were analyzed between every ten unknowns to check instrumental stability. ^{176}Hf/^{177}Hf ratios of the Mud Tank zircon gave an average of 0.2825355±0.0000041 (2SD; n=157); those of Temora gave 0.2826971±0.0000078 (2SD; n=51). These values are identical to those recommended for Mud Tank (0.282507±0.000003) and Temora (0.282693±0.000052) (Fisher et al. 2014). The isobaric interferences of ^{176}Lu and ^{176}Yb on ^{176}Hf are very limited, because of the extremely low ratios of Lu/Hf and Yb/Hf in the measured standard zircons. The interference of ^{176}Yb on ^{176}Hf was corrected by measuring the interference-free ^{172}Yb isotope and using ^{176}Yb/^{172}Yb to calculate ^{176}Yb/^{177}Hf. The appropriate value of ^{176}Yb/^{172}Yb was determined by successive spiking the JMC475 Hf standard (1 ppm solution) with Yb, and iteratively finding the value of ^{176}Yb/^{172}Yb required to yield the value of ^{176}Hf/^{177}Hf obtained on the pure Hf solution (Griffin et al. 2000; Griffin et al. 2004). Zircon Hf isotope data are presented in Table 5.

11. References

Abbo, A., Avigad, D., Gerdes, A. & Gungor, T. 2015. Cadomian basement and Paleozoic to Triassic siliciclastics of the Taurides (Karacahisar dome, south-central Turkey): Paleogeographic constraints from U-Pb-Hf in zircons. *Lithos*, **227**, 122-139.

Alavi, M. 2004. Regional stratigraphy of the Zagros fold-thrust belt of Iran and its proforeland evolution. *American Journal of Science*, **304**, 1-20.

Alavi, M. 2007. Structures of the Zagros fold-thrust belt in Iran. *American Journal of Science*, **307**, 1064-1095.

Angiolini, L., Zanchi, A., Zanchetta, S., Nicora, A. & Vezzoli, G. 2013. The Cimmerian geopuzzle: new data from South Pamir. *Terra Nova*, **25**, 352-360, http://doi.org/10.1111/ter.12042.

Atapour, H. & Aftabi, A. 2017a. Comments on "Geochronology and geochemistry of rhyolites from Hormuz Island, southern Iran: A new Cadomian arc magmatism in the Hormuz Formation" by N. S. Faramarzi, S. Amini, A. K. Schmitt, J. Hassanzadeh, G. Borg, K. McKeegan, S. M. H. Razavi, S. M. Mortazavi, Lithos, Sep. 2015, V.236-237, P.203-211: A missing link of Ediacaran A-type rhyolitic volcanism associated with glaciogenic banded iron salt formation (BISF). *Lithos*, **284**, 779-782, http://doi.org/10.1016/j.lithos.2016.07.043.

Atapour, H. & Aftabi, A. 2017b. The possible synglaciogenic Ediacaran hematitic banded iron salt formation (BISF) at Hormuz Island, southern Iran: Implications for a new style of exhalative hydrothermal iron-salt system. *Ore Geology Reviews*, **89**, 70-95, http://doi.org/10.1016/j.oregeorev.2017.05.033.

Avigad, D., Abbo, A. & Gerdes, A. 2016. Origin of the Eastern Mediterranean: Neotethys rifting along a cryptic Cadomian suture with Afro-Arabia. *Geological Society of America Bulletin*, **128**, 1286-1296, http://doi.org/10.1130/B31370.1.

Badr, M.J., Collins, A.S., Masoudi, F., Cox, G. & Mohajjel, M. 2013. The U-Pb age, geochemistry and tectonic significance of granitoids in the Soursat Complex, Northwest Iran. *Turkish Journal of Earth Sciences*, **22**, 1-31.

Baier, J., Audetat, A. & Keppler, H. 2008. The origin of the negative niobium tantalum anomaly in subduction zone magmas. *Earth and Planetary Science Letters*, **267**, 290-300.

Balaghi, M.E., Mahmoud, S., Zhai, M.G., Habibollah, G. & Mohammad, M. 2014. Zircon U-Pb ages, Hf isotopes and geochemistry of the schists, gneisses and granites in Delbar Metamorphic-Igneous Complex, SE of Shahrood (Iran): Implications for Neoproterozoic geodynamic evolutions of Central Iran. *Journal of Asian Earth Sciences*, **92**, 92-124.

Balaghi, Z., Sadeghian, M. & Ghasemi, H. 2010. Petrogenesis of the lower Paleozoic igneous rocks south of Bahabad (Bafq-Central Iran): Implication for rifting. *Petrology*, **4**, 45-64.

Belousova, E., Griffin, W.L., O'Reilly, S.Y. & Fisher, N. 2002. Igneous zircon: trace element composition as an indicator of source rock type. *Contributions to Mineralogy and Petrology*, **143**, 602-622.

Berberian, M. & King, G.C.P. 1981. Towards a Paleogeography and Tectonic Evolution of Iran. *Canadian Journal of Earth Sciences*, **18**, 210-265.

Bi, J.H., Ge, W.C., Yang, H., Wang, Z.H., Xu, W.L., Yang, J.H., Xing, D.H. & Chen, H.J. 2016. Geochronology and geochemistry of late Carboniferous-middle Permian I- and A-type granites and gabbro-diorites in the eastern Jiamusi Massif, NE China: Implications for petrogenesis and tectonic setting. *Lithos*, **266**, 213-232, http://doi.org/10.1016/j.lithos.2016.10.001.

Bowring, S.A., Grotzinger, J.P., Condon, D.J., Ramezani, J., Newall, M.J. & Allen, P.A. 2007. Geochronologic constraints on the chronostratigraphic framework of the neoproterozoic Huqf Supergroup, Sultanate of Oman. *American Journal of Science*, **307**, 1097-1145.

Chang, Z.S., Vervoort, J.D., McClelland, W.C. & Knaack, C. 2006. U-Pb dating of zircon by LA-ICP-MS. *Geochemistry Geophysics Geosystems*, **7**.

Crowley, Q.G., Floyd, P.A., Winchester, J.A., Franke, W. & Holland, J.G. 2000. Early Palaeozoic rift-related magmatism in Variscan Europe: fragmentation of the Armorican Terrane Assemblage. *Terra Nova*, **12**, 171-180.

Daneshvar, N., Maanijou, M., Azizi, H. & Asahara, Y. 2019. Petrogenesis and geodynamic implications of an Ediacaran (550 Ma) granite complex (metagranites), southwestern Saqqez, northwest Iran. *Journal of Geodynamics*, **132**, 101669.

Depaolo, D.J. 1981. Trace-Element and Isotopic Effects of Combined Wallrock Assimilation and Fractional Crystallization. *Earth and Planetary Science Letters*, **53**, 189-202, http://doi.org/Doi 10.1016/0012-821x(81)90153-9.

Ducea, M.N., Bergantz, G.W., Crowley, J.L. & Otamendi, J. 2017. Ultrafast magmatic buildup and diversification to produce continental crust during subduction. *Geology*, **45**, 235-238.

Ducea, M.N., Otamendi, J.E., Bergantz, G., Stair, K.M., Valencia, V.A. & Gehrels, G.E. 2010. Timing constraints on building an intermediate plutonic arc crustal section: U- Pb zircon geochronology of the Sierra Valle Fertil-La Huerta, Famatinian arc, Argentina. *Tectonics*, **29**.

Eby, G.N. 1992. Chemical subdivision of the A-type granitoids: petrogenetic and tectonic implications. *Geology*, **20**, 641-644.

Edgell, H.S. 1991. Proterozoic Salt Basins of the Persian Gulf Area and Their Role in Hydrocarbon Generation. *Precambrian Research*, **54**, 1-14.

Faramarzi, N.S., Amini, S., Schmitt, A.K., Hassanzadeh, J., Borg, G., McKeegan, K., Razavi, S.M.H. & Mortazavi, S.M. 2015. Geochronology and geochemistry of rhyolites from Hormuz Island, southern Iran: A new record of Cadomian arc magmatism in the Hormuz Formation. *Lithos*, **236**, 203-211, http://doi.org/10.1016/j.lithos.2015.08.017.

Fisher, C.M., Vervoort, J.D. & DuFrane, S.A. 2014. Accurate Hf isotope determinations of complex zircons using the "laser ablation split stream" method. *Geochemistry Geophysics Geosystems*, **15**, 121-139.

Griffin, W., Powell, W., Pearson, N. & O'reilly, S. 2008. GLITTER: data reduction software for laser ablation ICP-MS. *Laser Ablation-ICP-MS in the earth sciences. Mineralogical association of Canada short course series*, **40**, 204-207.

Griffin, W.L., Belousova, E.A., Shee, S.R., Pearson, N.J. & O'Reilly, S.Y. 2004. Archean crustal evolution in the northern Yilgam Craton: U-Pb and Hf-isotope evidence from detrital zircons. *Precambrian Research*, **131**, 231-282.

Griffin, W.L., Pearson, N.J., Belousova, E., Jackson, S.E., van Achterbergh, E., O'Reilly, S.Y. & Shee, S.R. 2000. The Hf isotope composition of cratonic mantle: LAM-MC-ICPMS analysis of zircon megacrysts in kimberlites. *Geochimica et Cosmochimica Acta*, **64**, 133-147, http://doi.org/Doi 10.1016/S0016-7037(99)00343-9.

Gursu, S., Moller, A., Goncuoglu, M.C., Koksal, S., Demircan, H., Koksal, F.T., Kozlu, H. & Sunal, G. 2015. Neoproterozoic continental arc volcanism at the northern edge of the Arabian Plate, SE Turkey. *Precambrian Research*, **258**, 208-233.

Hassanzadeh, J., Stockli, D.F., Horton, B.K., Axen, G.J., Stockli, L.D., Grove, M., Schmitt, A.K. & Walker, J.D. 2008. U-Pb zircon geochronology of late Neoproterozoic-Early Cambrian granitoids in Iran: Implications for paleogeography, magmatism, and exhumation history of Iranian basement. *Tectonophysics*, **451**, 71-96.

Hastie, A.R., Kerr, A.C., Pearce, J.A. & Mitchell, S.F. 2007. Classification of altered volcanic island arc rocks using immobile trace elements: Development of the Th-Co discrimination diagram. *Journal of Petrology*, **48**, 2341-2357, http://doi.org/DOI 10.1093/petrology/egm062.

Hildreth, W., Halliday, A.N. & Christiansen, R.L. 1991. Isotopic and Chemical Evidence Concerning the Genesis and Contamination of Basaltic and Rhyolitic Magma beneath the Yellowstone Plateau Volcanic Field. *Journal of Petrology*, **32**, 63-138.

Hofmann, A.W., Jochum, K., Seufert, M. & White, W.M. 1986. Nb and Pb in oceanic basalts: new constraints on mantle evolution. *Earth and Planetary Science Letters*, **79**, 33-45.

Honarmand, M., Xiao, W.J., Nabatian, G., Blades, M.L., dos Santos, M.C., Collins, A.S. & Ao, S.J. 2018. Zircon U-Pb-Hf isotopes, bulk-rock geochemistry and Sr-Nd-Pb isotopes from late Neoproterozoic basement in the Mahneshan area, NW Iran: Implications for Ediacaran active continental margin along the northern Gondwana and constraints on the late Oligocene crustal anatexis. *Gondwana Research*, **57**, 48-76, http://doi.org/10.1016/j.gr.2017.12.009.

Huang, H.Q., Li, X.H., Li, Z.X. & Li, W.X. 2013. Intraplate crustal remelting as the genesis of Jurassic high-K granites in the coastal region of the Guangdong Province, SE China. *Journal of Asian Earth Sciences*, **74**, 280-302.

Hughes, N.C., Myrow, P.M., Ghazi, S., McKenzie, N.R., Stockli, D.F. & DiPietro, J.A. 2019. Cambrian geology of the Salt Range of Pakistan: Linking the Himalayan margin to the Indian craton. *Bulletin*, **131**, 1095-1114.

Husseini, M.I. 1992. Upper Paleozoic Tectonosedimentary Evolution of the Arabian and Adjoining Plates. *Journal of the Geological Society*, **149**, 419-429, http://doi.org/DOI 10.1144/gsjgs.149.3.0419.

Husseini, M.I. & Husseini, S.I. 1990. Origin of the Infracambrian salt basins of the Middle East. *Geological society, london, special publications*, **50**, 279-292.

Jackson, S.E., Pearson, N.J., Griffin, W.L. & Belousova, E.A. 2004. The application of laser ablation-inductively coupled plasma-mass spectrometry to in situ U-Pb zircon geochronology. *Chemical Geology*, **211**, 47-69.

Jahani, S., Callot, J.-P., de Lamotte, D.F., Letouzey, J. & Leturmy, P. 2007. The salt diapirs of the eastern Fars Province (Zagros, Iran): A brief outline of their past and present *Thrust Belts and Foreland Basins*. Springer, 289-308.

Kent, P.E. 1958. Recent studies of south Persian salt diapirs. *Association of Petroleum Geologists Bulletin*, **42**, 2951-2972.

Kent, P.E. 1979. The emergent Hormuz salt diapirs of southern Iran. *Journal of Petroleum Geology*, **2**, 117-144.

Kepezhinskas, P., Defant, M.J. & Drummond, M.S. 1996. Progressive enrichment of island arc mantle by melt-peridotite interaction inferred from Kamchatka xenoliths. *Geochimica Et Cosmochimica Acta*, **60**, 1217-1229.

Linnemann, U., Gerdes, A., Hofmann, M. & Marko, L. 2014. The Cadomian Orogen: Neoproterozoic to Early Cambrian crustal growth and orogenic zoning along the periphery of the West African Craton-Constraints from U-Pb zircon ages and Hf isotopes (Schwarzburg Antiform, Germany). *Precambrian Research*, **244**, 236-278.

Ludwig, K.R. 2003. *User's Manual for Isoplot 3.00: A Geochronological Toolkit for Microsoft Excel*.

Maleki, L., Rashidnejad-e-Omran, N. & Hooshmandzadeh, A. 2019. Petrology, geochemistry and Sr-Nd isotopic composition of the metabasic rocks of

Boneh shurow metamorphic complex, East of Saghand, Central Iran. *Scientific Quarterly Journal, Geosciences*, **29**, 196-185.

Mattes, B. & Morris, S.C. 1990. Carbonate/evaporite deposition in the Late Precambrian—Early Cambrian Ara Formation of Southern Oman. *Geological Society, London, Special Publications*, **49**, 617-636.

Miskovic, A. & Schaltegger, U. 2009. Crustal growth along a non-collisional cratonic margin: A Lu-Hf isotopic survey of the Eastern Cordilleran granitoids of Peru. *Earth and Planetary Science Letters*, **279**, 303-315, http://doi.org/10.1016/j.epsl.2009.01.002.

Moghadam, H.S., Corfu, F., Stern, R.J. & Lotfi Bakhsh, A. 2019. The Eastern Khoy metamorphic complex of NW Iran: a Jurassic ophiolite or continuation of the Sanandaj–Sirjan Zone? *Journal of the Geological Society*, http://doi.org/10.1144/jgs2018-081.

Moghadam, H.S., Khademi, M., Hu, Z.C., Stern, R.J., Santos, J.F. & Wu, Y.B. 2015. Cadomian (Ediacaran-Cambrian) arc magmatism in the ChahJam-Biarjmand metamorphic complex (Iran): Magmatism along the northern active margin of Gondwana. *Gondwana Research*, **27**, 439-452, http://doi.org/10.1016/j.gr.2013.10.014.

Moghadam, H.S., Li, X.H., Stern, R.J., Santos, J.F., Ghorbani, G. & Pourmohsen, M. 2016. Age and nature of 560-520 Ma calc-alkaline granitoids of Biarjmand, northeast Iran: insights into Cadomian arc magmatism in northern Gondwana. *International Geology Review*, **58**, 1492-1509, http://doi.org/10.1080/00206814.2016.1166461.

Moghadam, H.S., Li, X.H., Santos, J.F., Stern, R.J., Griffin, W.L., Ghorbani, G. & Sarebani, N. 2017a. Neoproterozoic magmatic flare-up along the N. margin of Gondwana: The Taknar complex, NE Iran. *Earth and Planetary Science Letters*, **474**, 83-96, http://doi.org/10.1016/j.epsl.2017.06.028.

Moghadam, H.S., Li, X.-H., Santos, J.F., Stern, R.J., Griffin, W.L., Ghorbani, G. & Sarebani, N. 2017b. Neoproterozoic magmatic flare-up along the N. margin of Gondwana: The Taknar complex, NE Iran. *Earth and Planetary Science Letters*, **474**, 83-96, http://doi.org/10.1016/j.epsl.2017.06.028.

Moghadam, H.S., Li, Q.L., Griffin, W.L., Stern, R.J., Ishizuka, O., Henry, H., Lucci, F., O'Reilly, S.Y., *et al.* 2020. Repeated magmatic buildup and deep "hot zones" in continental evolution: The Cadomian crust of Iran. *Earth and Planetary Science Letters*, **531**, http://doi.org/ARTN 115989 10.1016/j.epsl.2019.115989.

Moghadam, H.S., Griffin, W.L., Li, X.H., Santos, J.F., Karsli, O., Stern, R.J., Ghorbani, G., Gain, S., *et al.* 2017c. Crustal Evolution of NW Iran: Cadomian Arcs, Archean Fragments and the Cenozoic Magmatic Flare-Up. *Journal of Petrology*, **58**, 2143-2190, http://doi.org/10.1093/petrology/egy005.

Momenzadeh, M. & Heidari, E. 1995. Ore-hydrocarbon resources and alkaline magmatism of Late Proterozoic-Early Cambrian in Iran: A genetic interpretation. *Carbonates and Evaporites*, **10**, 79-88.

Mouthereau, F., Lacombe, O. & Verges, J. 2012. Building the Zagros collisional orogen: Timing, strain distribution and the dynamics of Arabia/Eurasia plate convergence. *Tectonophysics*, **532**, 27-60.

Nance, R.D. & Murphy, J.B. 1994. Contrasting Basement Isotopic Signatures and the Palinspastic Restoration of Peripheral Orogens - Example from the Neoproterozoic Avalonian-Cadomian Belt. *Geology*, **22**, 617-620.

Nelson, S.T. & Montana, A. 1992. Sieve-textured plagioclase in volcanic rocks produced by rapid decompression. *American Mineralogist*, **77**, 1242-1249.

Neubauer, F., Klotzli, U.S. & Poscheschnik, P. 2001. Cadomian magmatism in the Alps recorded in Late Ordovician sandstones of the Carnic Alps: preliminary results from zircon Pb/Pb evaporation dating. *Schweizerische Mineralogische Und Petrographische Mitteilungen*, **81**, 175-179.

Ottley, C., Pearson, D. & Irvine, G. 2003. A routine method for the dissolution of geological samples for the analysis of REE and trace elements via ICP-MS. *Plasma source mass spectrometry: Applications and emerging technologies*, 221.

Pearce, J.A. & Peate, D.W. 1995a. Tectonic implications of the composition of volcanic arc magmas. *Annual Review of Earth and Planetary Sciences*, **23**, 251-285.

Pearce, J.A. & Peate, D.W. 1995b. Tectonic Implications of the Composition of Volcanic Arc Magmas. *Annual Review of Earth and Planetary Sciences*, **23**, 251-285.

Pearce, J.A., Harris, N.B. & Tindle, A.G. 1984. Trace element discrimination diagrams for the tectonic interpretation of granitic rocks. *Journal of Petrology*, **25**, 956-983.

Pereira, M.F., Chichorro, M., Sola, A.R., Silva, J.B., Sanchez-Garcia, T. & Bellido, F. 2011. Tracing the Cadomian magmatism with detrital/inherited zircon ages by in-situ U-Pb SHRIMP geochronology (Ossa-Morena Zone, SW Iberian Massif). *Lithos*, **123**, 204-217.

Potts, P.J., Tindle, A.G. & Webb, P. 1992. *Geochemical reference material compositions: rocks, minerals, sediments, soils, carbonates, refractories & ores used in research & industry*. Taylor & Francis.

Ramezani, J. & Tucker, R.D. 2003. The Saghand Region, Central Iran: U-Pb geochronology, petrogenesis and implications for Gondwana Tectonics. *American Journal of Science*, **303**, 622-665, http://doi.org/DOI 10.2475/ajs.303.7.622.

Rudnick, R.L. 1992. Restites, Eu Anomalies, and the Lower Continental-Crust. *Geochimica Et Cosmochimica Acta*, **56**, 963-970.

Rudnick, R.L. 1995. Making Continental-Crust. *Nature*, **378**, 571-578.

Sepidbar, F., Shafaii Moghadam, H., Li, C., Stern, R.J., Jiantang, P. & Vesali, Y. revised. Cadomian Magmatic Rocks from Zarand (SE Iran) Formed in a Retro-Arc Basin. *Lithos*.

Shabanian, N., Davoudian, A.R., Dong, Y.P. & Liu, X.M. 2018. U-Pb zircon dating, geochemistry and Sr-Nd-Pb isotopic ratios from Azna-Dorud Cadomian metagranites, Sanandaj-Sirjan Zone of western Iran. *Precambrian Research*, **306**, 41-60, http://doi.org/10.1016/j.precamres.2017.12.037.

Shafaii Moghadam, H., Li, Q.L., Griffin, W.L., Stern, R.J., Ishizuka, O., Henry, H., Lucci, F., O'Reilly, S.Y., *et al.* 2020. Repeated magmatic buildup and deep "hot zones" in continental evolution: The Cadomian crust of Iran. *Earth and Planetary Science Letters*, **531**, http://doi.org/10.1016/j.epsl.2019.115989.

Shakerardakani, F., Neubauer, F., Masoudi, F., Mehrabi, B., Liu, X.M., Dong, Y.P., Mohajjel, M., Monfaredi, B., *et al.* 2015. Panafrican basement and Mesozoic gabbro in the Zagros orogenic belt in the Dorud-Azna region (NW Iran): Laser-ablation ICP-MS zircon ages and geochemistry. *Tectonophysics*, **647**, 146-171, http://doi.org/10.1016/j.tecto.2015.02.020.

Stern, R.J., Ali, K.A., Abdelsalam, M.G., Wilde, S.A. & Zhou, Q. 2012. U-Pb zircon geochronology of the eastern part of the Southern Ethiopian Shield. *Precambrian Research*, **206**, 159-167.

Stocklin, J. 1968. Structural history and tectonics of Iran, A review. *Aapg Bulletin*, **52**, 1229-1258.

Sun, S.-S. & McDonough, W.-s. 1989. Chemical and isotopic systematics of oceanic basalts: implications for mantle composition and processes. *Geological society, london, special publications*, **42**, 313-345.

Taghipour, S., Khalili, M., Mackizadeh, M.A., Kananian, A. & Taghipour, B. 2013. Mineralogy, geochemistry and petrogenesis of igneous inclusions within three inactive diapirs, Zagros belt, Shahre-kord, Iran. *Geological Magazine*, **150**, 72-88.

Talbot, C. & Alavi, M. 1996. The past of a future syntaxis across the Zagros. *Geological society, london, special publications*, **100**, 89-109.

Talbot, C., Aftabi, P. & Chemia, Z. 2009a. Potash in a salt mushroom at Hormoz island, Hormoz strait, Iran. *Ore Geology Reviews*, **35**, 317-332.

Talbot, C.J., Farhadi, R. & Aftabi, P. 2009b. Potash in salt extruded at Sar Pohl diapir, Southern Iran. *Ore Geology Reviews*, **35**, 352-366, http://doi.org/DOI 10.1016/j.oregeorev.2008.11.002.

Thomas, R.J., Ellison, R.A., Goodenough, K.M., Roberts, N.M.W. & Allen, P.A. 2015. Salt domes of the UAE and Oman: Probing eastern Arabia. *Precambrian Research*, **256**, 1-16.

Tindle, A.G. & Pearce, J.A. 1983. Assimilation and Partial Melting of Continental-Crust - Evidence from the Mineralogy and Geochemistry of Autoliths and Xenoliths. *Lithos*, **16**, 185-202.

Ustaomer, P.A., Ustaomer, T., Collins, A.S. & Robertson, A.H.F. 2009. Cadomian (Ediacaran-Cambrian) arc magmatism in the Bitlis Massif, SE Turkey: Magmatism along the developing northern margin of Gondwana. *Tectonophysics*, **473**, 99-112.

Veiskarami, M., Sadeghian, M., Mingguo, M. & Ghasemi, H. 2019. Petrology, geochemistry and dating of the Late Neoproterozoic metabasites of the Majerad metamorphic complex (SE Shahrood): One step for understanding the geodynamic evolutions of Iranian Gondawanan terranes. *Iranian Journal of Crystallography and Mineralogy*, **27**, 191-206.

von Raumer, J.F., Stampfli, G.M., Borel, G. & Bussy, F. 2002. Organization of pre-Variscan basement areas at the north-Gondwanan margin. *International Journal of Earth Sciences*, **91**, 35-52.

Wang, R.R., Xu, Z.Q., Santosh, M., Yao, Y., Gao, L.E. & Liu, C.H. 2016. Late Neoproterozoic magmatism in South Qinling, Central China: Geochemistry, zircon U-Pb-Lu-Hf isotopes and tectonic implications. *Tectonophysics*, **683**, 43-61, http://doi.org/10.1016/j.tecto.2016.05.050.

Whalen, J.B., Currie, K.L. & Chappell, B.W. 1987. A-type granites: geochemical characteristics, discrimination and petrogenesis. *Contributions to Mineralogy and Petrology*, **95**, 407-419.

Woodhead, J.D. & Hergt, J.M. 2005. A preliminary appraisal of seven natural zircon reference materials for in situ Hf isotope determination. *Geostandards and Geoanalytical Research*, **29**, 183-195.

Yuan, H.L., Gao, S., Dai, M.N., Zong, C.L., Gunther, D., Fontaine, G.H., Liu, X.M. & Diwu, C. 2008. Simultaneous determinations of U-Pb age, Hf isotopes and trace element compositions of zircon by excimer laser-ablation quadrupole and multiple-collector ICP-MS. *Chemical Geology*, **247**, 100-118.

Zindler, A. & Hart, S. 1986. Chemical geodynamics. *Annual Review of Earth and Planetary Sciences*, **14**, 493-571.

Zulauf, G., Dorr, W., Fiala, J. & Vejnar, Z. 1997. Late Cadomian crustal tilting and Cambrian transtension in the Tepla-Barrandian unit (Bohemian Massif, Central European Variscides). *Geologische Rundschau*, **86**, 571-584.

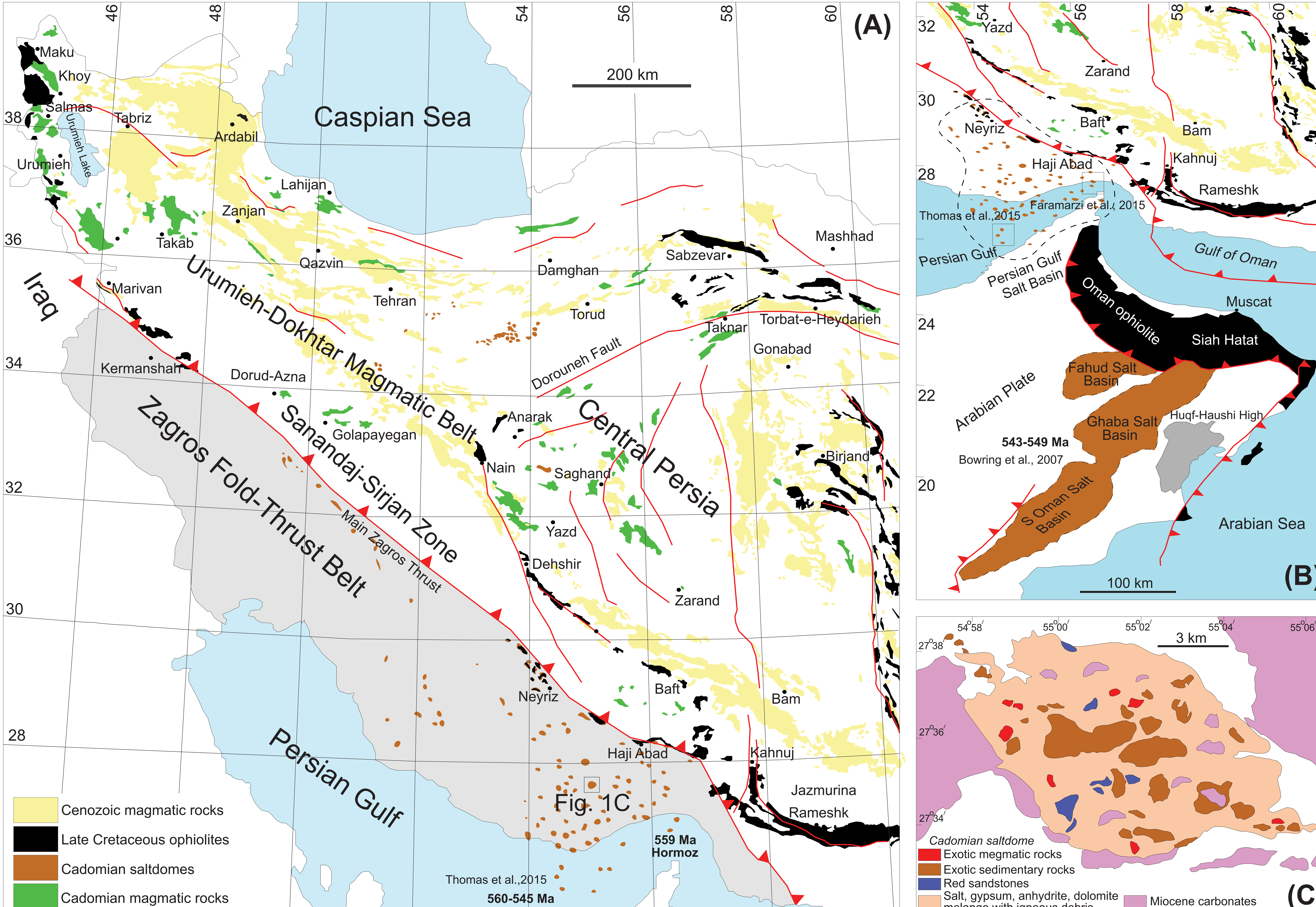
(A)
Caspian Sea
200 km
Maku
Khoy
Salmas
Tabriz
Urumieh Lake
Ardabil
Urumieh
Lahijan
Zanjan
Takab
Qazvin
Tehran
Damghan
Sabzevar
Mashhad
Iraq
Marivan
Urumieh-Dokhtar Magmatic Belt
Torud
Taknar
Torbat-e-Heydarieh
Gonabad
Doruneh Fault
Kermanshah
Dorud-Azna
Golapayegan
Anarak
Nain
Saghand
Central Persia
Birjand
Zagros Fold-Thrust Belt
Sanandaj-Sirjan Zone
Main Zagros Thrust
Yazd
Dehshir
Zarand
Neyriz
Baft
Bam
Haji Abad
Kahnuj
Jazmurina
Rameshk
Fig. 1C
Persian Gulf
559 Ma
Hormoz
Thomas et al.,2015
560-545 Ma
Cenozoic magmatic rocks
Late Cretaceous ophiolites
Cadomian saltdomes
Cadomian magmatic rocks
(B)
Yazd
Zarand
Neyriz
Baft
Bam
Kahnuj
Haji Abad
Rameshk
Faramarzi et al., 2015
Thomas et al.,2015
Persian Gulf
Persian Gulf Salt Basin
Gulf of Oman
Muscat
Oman ophiolite
Siah Hatat
Fahud Salt Basin
Arabian Plate
Ghaba Salt Basin
Huqf-Haushi High
543-549 Ma
Bowring et al., 2007
S Oman Salt Basin
Arabian Sea
100 km
(C)
3 km
Cadomian saltdome
Exotic megmatic rocks
Exotic sedimentary rocks
Red sandstones
Salt, gypsum, anhydrite, dolomite melange with igneous debris
Miocene carbonates

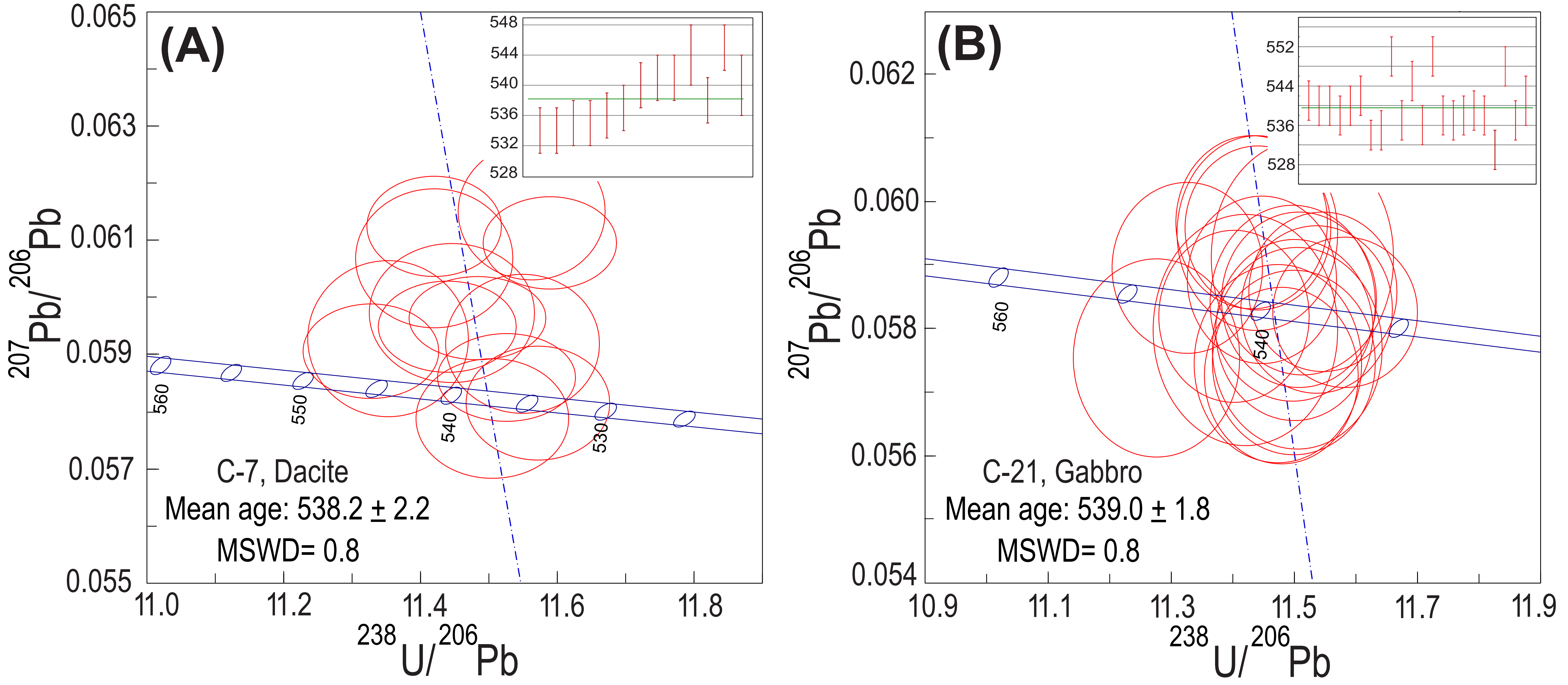
(A)
C-7, Dacite
Mean age: 538.2 ± 2.2
MSWD= 0.8
(B)
C-21, Gabbro
Mean age: 539.0 ± 1.8
MSWD= 0.8
207Pb/206Pb
238U/206Pb
560
550
540
530

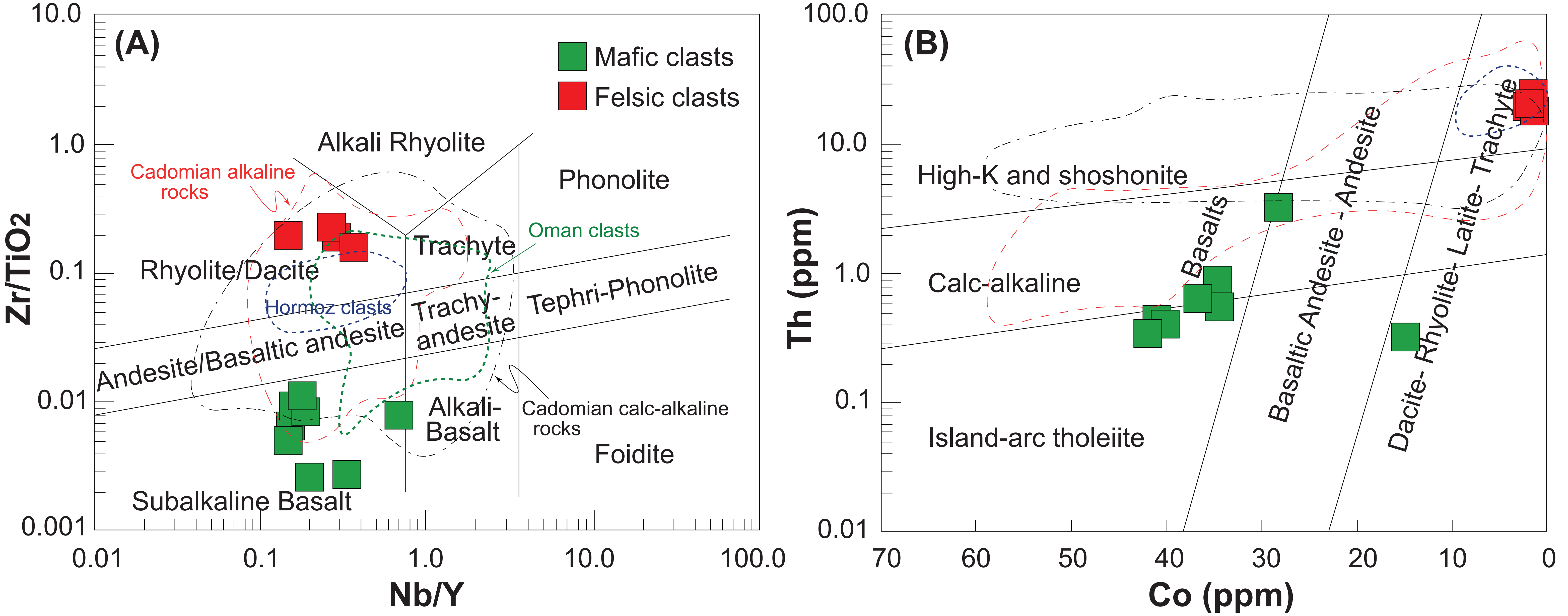
(A)
Mafic clasts
Felsic clasts
Alkali Rhyolite
Phonolite
Cadomian alkaline rocks
Oman clasts
Trachyte
Rhyolite/Dacite
Hormoz clasts
Trachy-andesite
Tephri-Phonolite
Andesite/Basaltic andesite
Cadomian calc-alkaline rocks
Alkali-Basalt
Foidite
Subalkaline Basalt
Zr/TiO2
Nb/Y
10.0
1.0
0.1
0.01
0.001
0.01
0.1
1.0
10.0
100.0
(B)
High-K and shoshonite
Calc-alkaline
Island-arc tholeiite
Basalts
Basaltic Andesite - Andesite
Dacite- Rhyolite- Latite- Trachyte
Th (ppm)
Co (ppm)
100.0
10.0
1.0
0.1
0.01
70
60
50
40
30
20
10
0

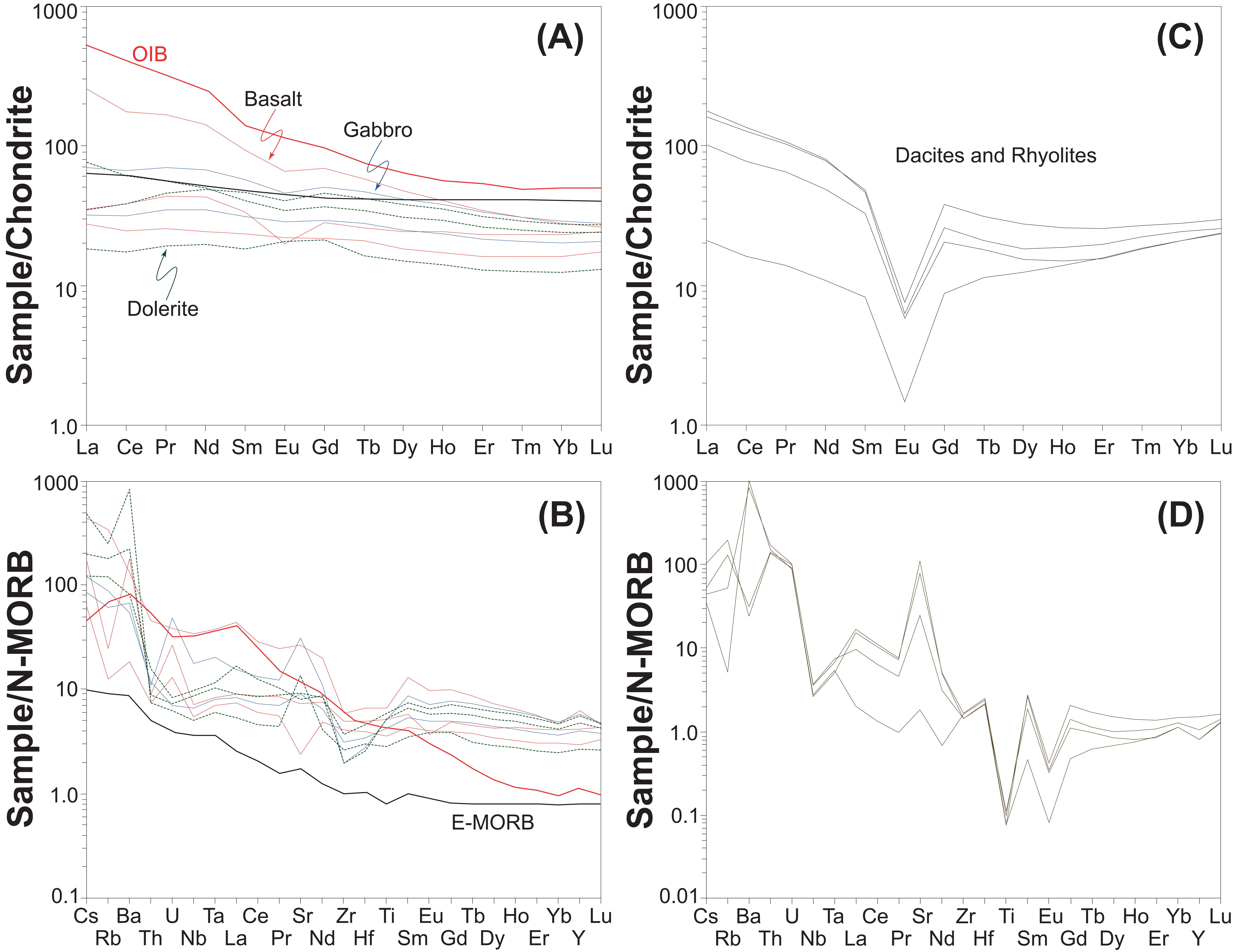

(A)
OIB
Basalt
Gabbro
Dolerite
Sample/Chondrite
1000
100
10
1.0
La Ce Pr Nd Sm Eu Gd Tb Dy Ho Er Tm Yb Lu
(C)
Dacites and Rhyolites
Sample/Chondrite
(B)
E-MORB
Sample/N-MORB
0.1
Cs Rb Ba Th U Nb Ta La Ce Pr Sr Nd Zr Hf Ti Sm Eu Gd Tb Dy Ho Er Yb Y Lu
(D)
Sample/N-MORB
0.01

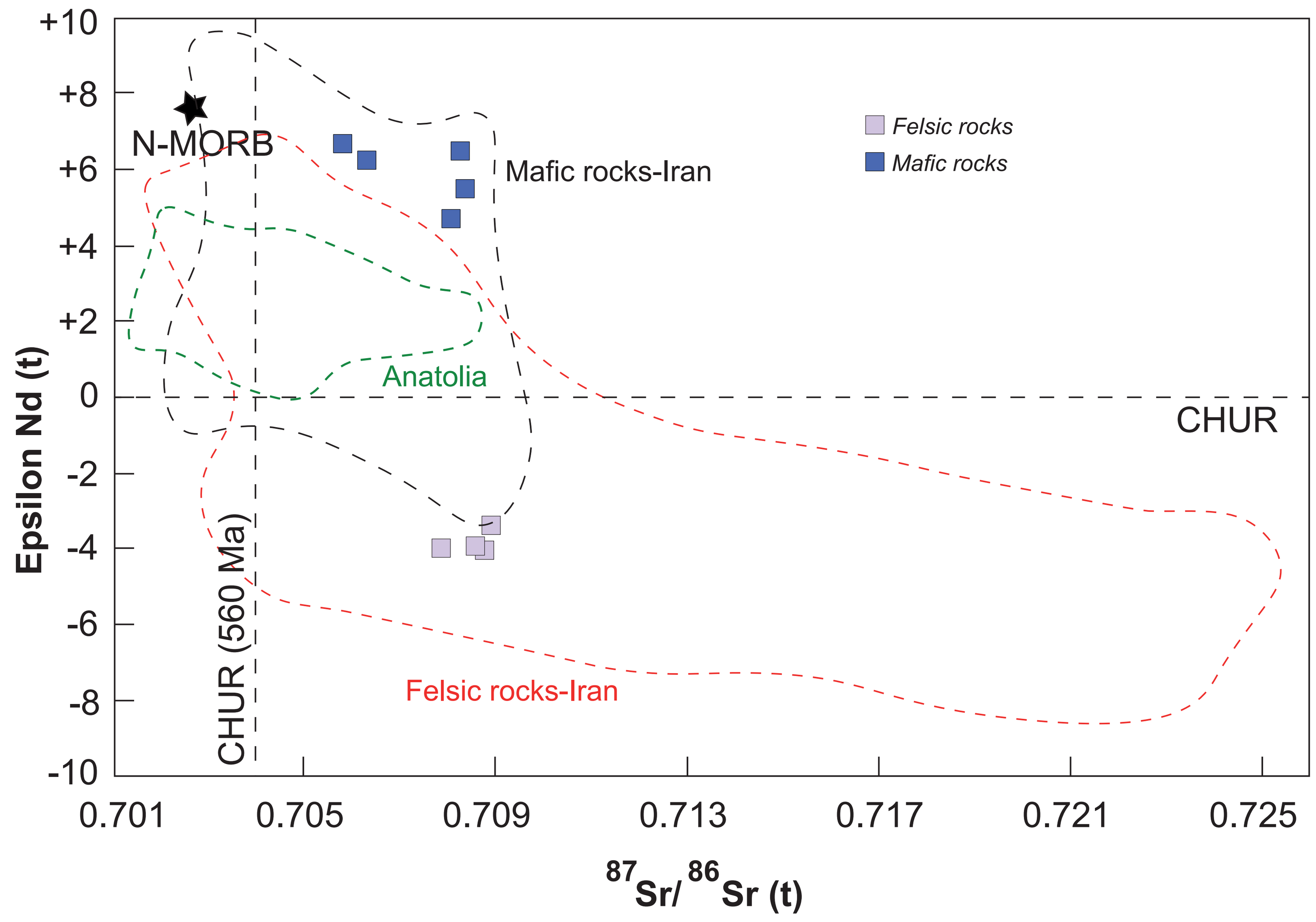

+10
+8
+6
+4
+2
0
-2
-4
-6
-8
-10
Epsilon Nd (t)
N-MORB
Mafic rocks-Iran
Felsic rocks
Mafic rocks
Anatolia
CHUR
CHUR (560 Ma)
Felsic rocks-Iran
0.701
0.705
0.709
0.713
0.717
0.721
0.725
87Sr/86Sr (t)

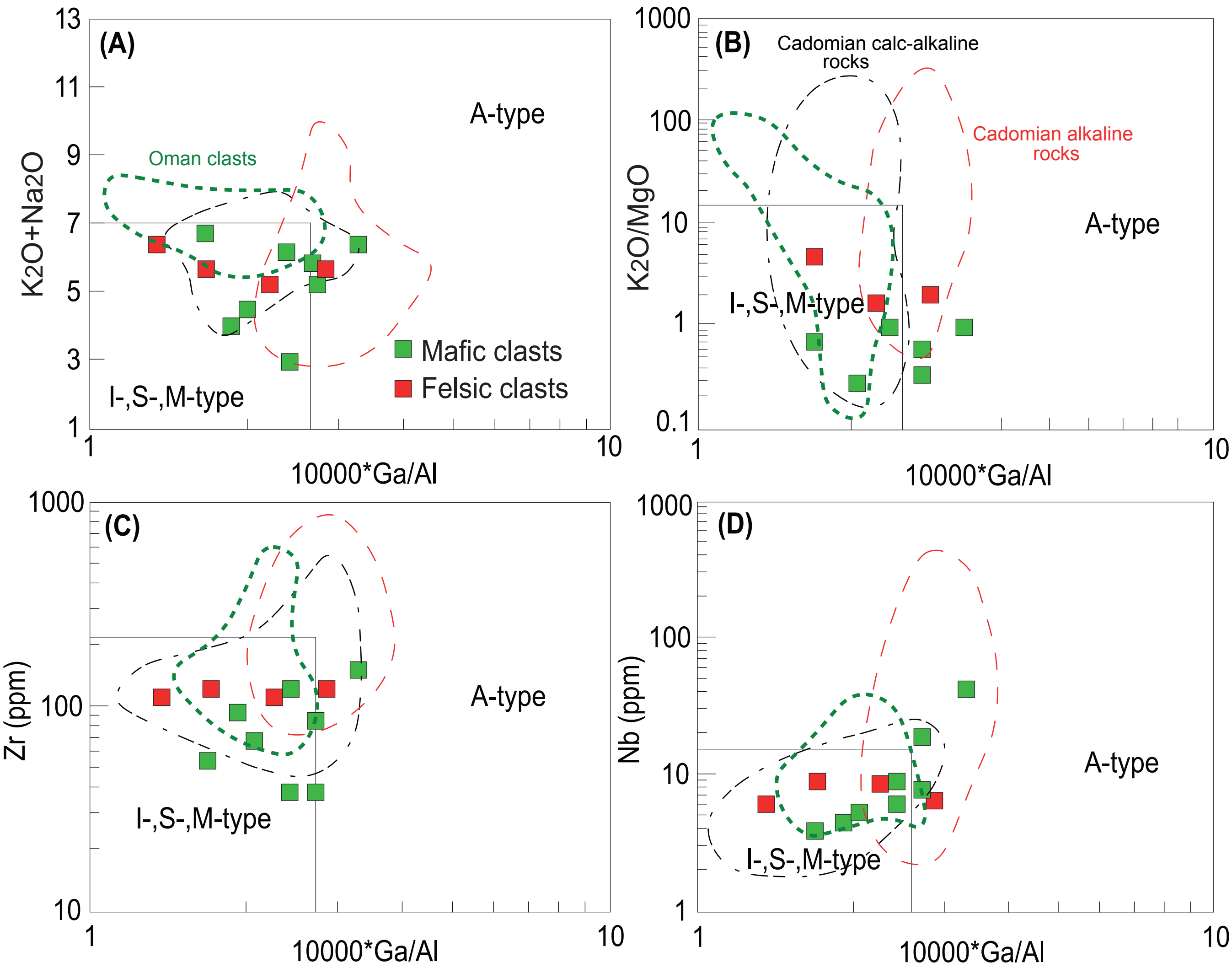

(A)
A-type
Oman clasts
I-,S-,M-type
Mafic clasts
Felsic clasts
K2O+Na2O
10000*Ga/Al
(B)
Cadomian calc-alkaline rocks
Cadomian alkaline rocks
A-type
I-,S-,M-type
K2O/MgO
10000*Ga/Al
(C)
A-type
I-,S-,M-type
Zr (ppm)
10000*Ga/Al
(D)
A-type
I-,S-,M-type
Nb (ppm)
10000*Ga/Al

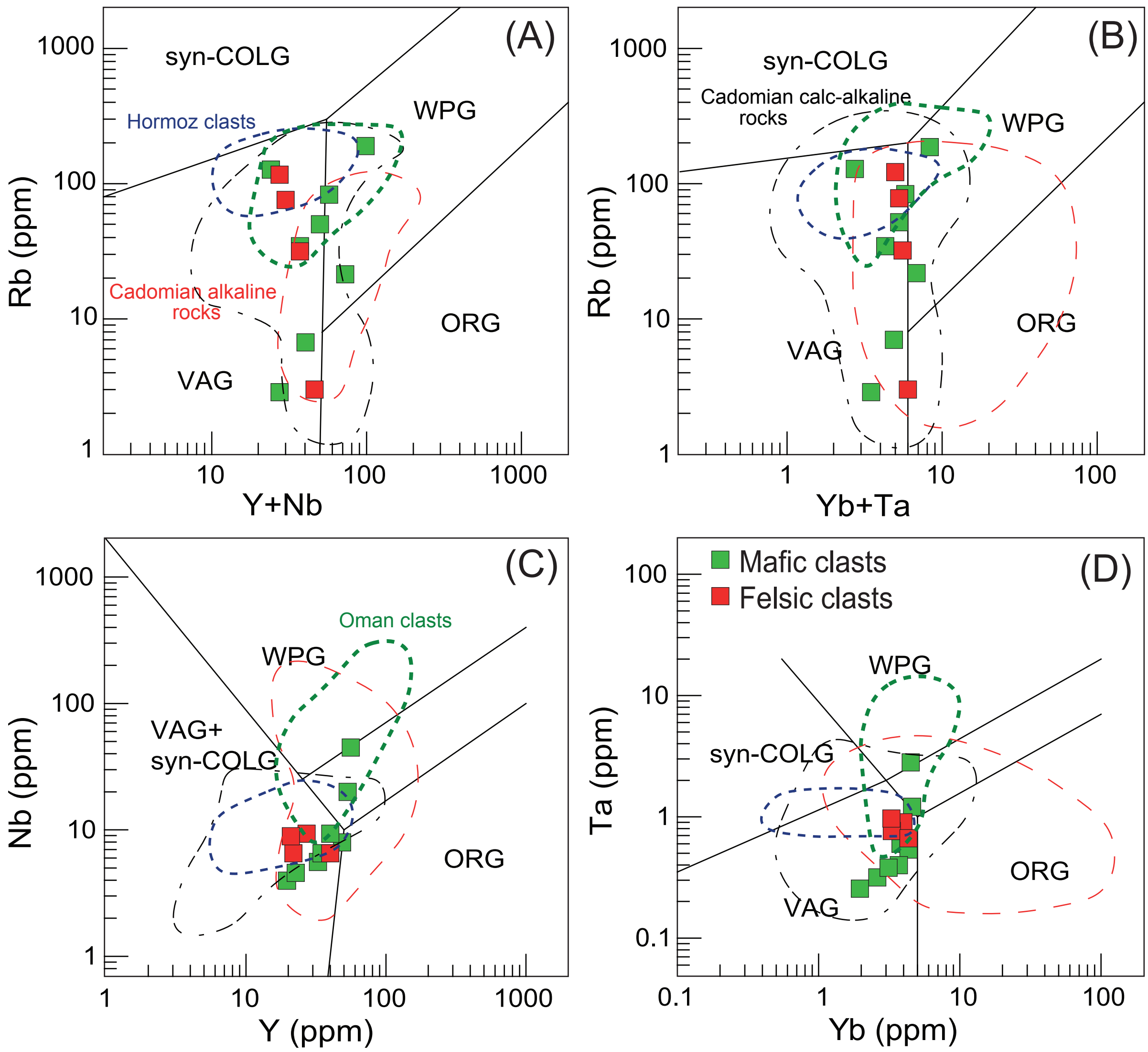

(A)
syn-COLG
Hormoz clasts
WPG
Cadomian alkaline rocks
VAG
ORG
Rb (ppm)
Y+Nb
1000
100
10
1
10
100
1000
(B)
syn-COLG
Cadomian calc-alkaline rocks
WPG
VAG
ORG
Rb (ppm)
Yb+Ta
1000
100
10
1
1
10
100
(C)
Oman clasts
WPG
VAG+
syn-COLG
ORG
Nb (ppm)
Y (ppm)
1000
100
10
1
1
10
100
1000
(D)
Mafic clasts
Felsic clasts
WPG
syn-COLG
VAG
ORG
Ta (ppm)
Yb (ppm)
100
10
1
0.1
0.1
1
10
100

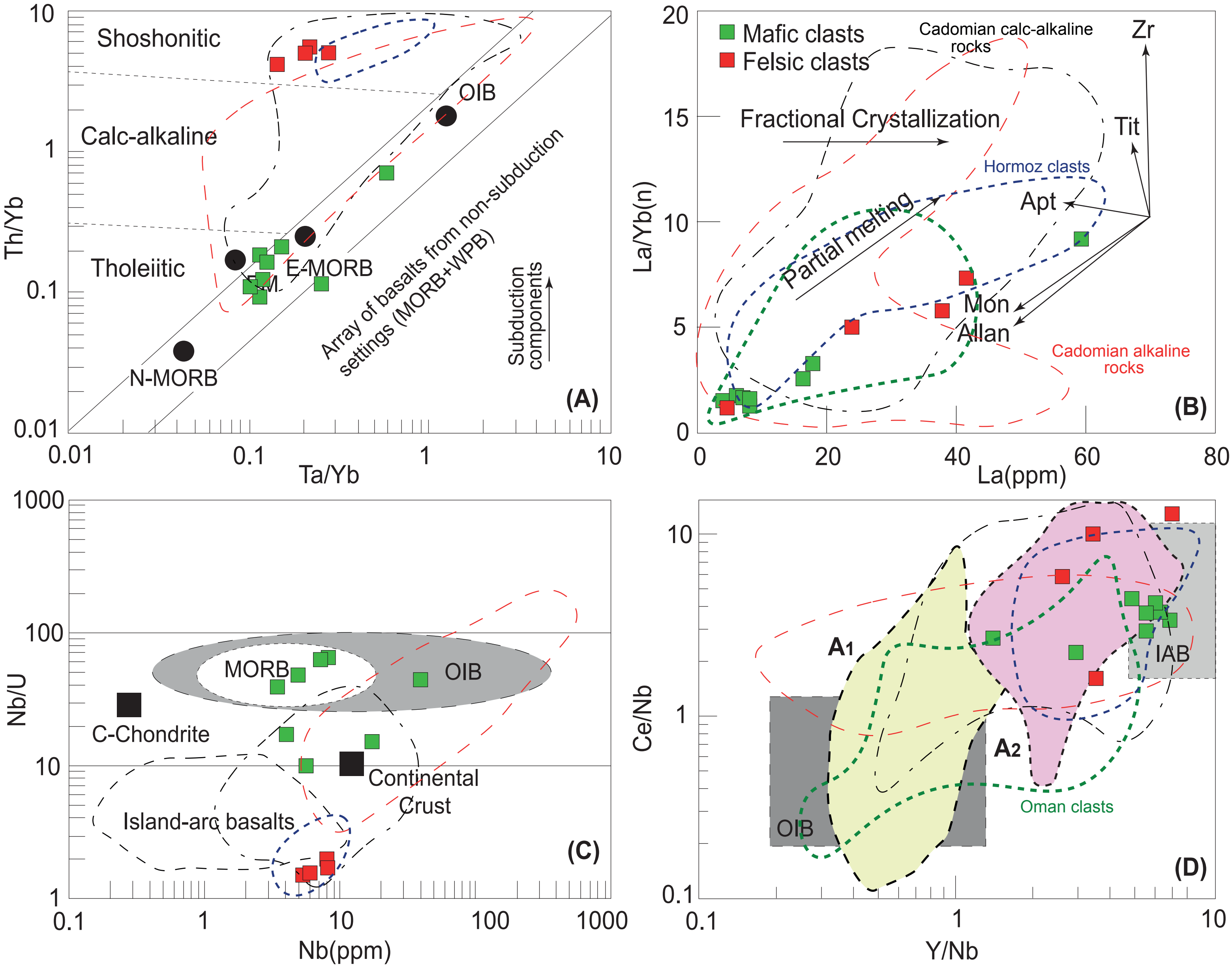
Shoshonitic
Calc-alkaline
Tholeiitic
OIB
E-MORB
N-MORB
Array of basalts from non-subduction settings (MORB+WPB)
Subduction components
Th/Yb
Ta/Yb
(A)
Mafic clasts
Felsic clasts
Cadomian calc-alkaline rocks
Zr
Tit
Fractional Crystallization
Hormoz clasts
Apt
Partial melting
Mon
Allan
Cadomian alkaline rocks
La/Yb(n)
La(ppm)
(B)
MORB
OIB
C-Chondrite
Continental Crust
Island-arc basalts
Nb/U
Nb(ppm)
(C)
A1
A2
IAB
OIB
Oman clasts
Ce/Nb
Y/Nb
(D)